Stagnant Motions in Hamiltonian Systems

Yoji AIZAWA, Yasuhiro KIKUCHI, Takahisa HARAYAMA
Kenshi YAMAMOTO, Motonori OTA and Kenji TANAKA

Department of Applied Physics, Waseda University, Tokyo 169

(Received April 5, 1989)

Hamiltonian systems often reveal the chaotic phenomena with long time memory, and then the time average of a dynamical variable does not seem to converge toward a certain constant monotonically. Even when the time average looks like a constant in the limit under a given initial condition, for many cases the limiting value often depends sensitively on the initial data. Chaos in the dynamical system is usually discussed in the framework of the ergodic theory which guarantees the weak law of the large number and the unique existence of the time average except for the measure zero set. However, the hamiltonian chaos seems to be difficult to understand on the same line straightforwardly. The essence of the hamiltonian chaos seems to be more complex (or robust) than that of the purely ergodic ones. In this paper we devote ourselves to the research of the origin of such wild long time tails.

A result of our phenomenological approaches is that the hamiltonian chaos is non-stationary and multi-ergodic. The various effects of the long time tails such as the f^{-2} spectrum and the anomalous large deviation will be explained from a universality law in the transition regime between chaos and torus.

Contents

§ 1. Introduction

The dominant structures in the hamiltonian dynamics are *chaos and torus.* The main concern of the present paper is to elucidate the general features in the transition regime between chaos and torus (or between the probability and the deterministics). The basic problems of chaos in hamiltonian systems will be surveyed from that concern.

1.1. *Between chaos and torus ——Twilight zone of causality——*

Chaos in the hamiltonian system was noticed by Poincaré for the first time in the study of the 3-body problem of celestial mechanics.[1] He explained the onset mechanism of chaos in terms of the transverse homoclinicity (or heteroclinicity), which implies the orbital instability due to a special geometrical structure of invariant manifolds in phase space. The analytical condition for the creation of such special structures was formulated later by Mel'nikov in 1963,[2] and that was successfully used by Arnold in 1964 to predict the characteristic features of the chaotic region so-called *instability zone.*[3] It was proved by Smale in 1967 that the content of the instability zone is quite rich and even a variety of random motions are generated therein.[4]

When the transversality of the stable and unstable foliations are satisfied everywhere in phase space, the instability zone becomes a strong ergodic set, where the Anosov-Sinai theorem can be applied to determine the characteristics of the system such as entropy, Lyapunov exponent, etc. (see § 1.4).[5)~8)] But in the large class of hamiltonian systems, the transversality is violated and the tangential homoclinicity (or heteroclinicity) may appear in general. When the orbital instability is lost owing to the tangential homoclinicity, the orbit is eventually confined only into a lower dimensional hypersurface in phase space, i.e., a lot of chaotic orbits come out to degenerate on a low dimensional manifold with less symmetry. After such degeneracy happens, what kinds of manifolds are generally induced? It is known that the most dominant one of them is a torus, if the system is bounded and the phase space is compact.

The torus is an especially important structure in hamiltonian dynamics. The Liouville-Arnold theorem states that if the bounded hamiltonian is integrable by quadrature, almost every orbit is generically confined in each inherent torus and whole space are densely covered by tori.[9] Then the hamiltonian $H(\boldsymbol{P}, \boldsymbol{Q})$ is separable,

$$H(\boldsymbol{P}, \boldsymbol{Q})=\sum_i H_i(P_i, Q_i)\,, \tag{1·1}$$

where $\boldsymbol{P}=(P_1, P_2, \cdots, P_n)$ and $\boldsymbol{Q}=(Q_1, Q_2, \cdots, Q_n)$ are canonical $2n$ variables. Therefore we can say that when chaos is destroyed by the tangential homoclinicity, a locally integrable sub-set (or torus) can be created in phase space. Conversely, when the torus is demolished under the Mel'nikov condition for the transversal homoclinicity, the instability zone (or chaos) can be released. Generally speaking, chaos and torus are simultaneously coexisting, and both are alternative at every point in phase space.[29)~38)]

The transition from chaos to torus is believed to be a "all-or-none" type, but a question is whether the transition regime exists between chaos and torus. The torus region is considered to be a stable phase which has a long range order in time, but chaos region to be an unstable phase that has only a short range temporal order. If there is a certain transition layer between chaos and torus, the motion in such layer must reveal a partial order with multi-time scales. The main purpose of the present paper is to examine the uncertainty phenomena concealed in such twilight zone between chaos and torus. The analogy with the critical phenomena in statistical mechanics will be discussed for several topics in the latter sections.

The dynamical system is always subjected to a certain deterministic law of causality, e.g., under a given hamiltonian. However, such causality in law becomes impotent in the long time prediction of a chaotic orbit, since the causality is not decomposable in the sense of Eq. (1·1), and we only know the probability of the orbital distribution in the sense of ergodic ensemble. Namely, the causality in law enables us to predict only the short time behavior for a chaotic orbit. Thus the transition from chaos to torus is the twilight zone of causality.

1.2. *Stability of torus ——Analytical approach——*

The stability of a torus is examined by introducing the perturbation into the system given by Eq. (1·1). Under an appropriate canonical transformation, the hamiltonian is generally rewritten into,

$$H(p, q, \varepsilon)=H_0(p)+\varepsilon H_1(p, q)\,, \tag{1·2}$$

where (p, q) are the action-angle variables and ε is a perturbation parameter.

The Poincaré theorem states that there is no uniform integral in this system except for the hamiltonian $H(p, q, \varepsilon)$ itself.[10)] The *uniform integral* means the one-valued analytic global constant of motion, which is often called the isolating global integral.[11)] The Poincaré theorem suggests that the more unstable and complex motions than the torus can be created in the nearly integrable system of Eq. (1·2). Based on this theorem in 1923 Fermi tried to prove the ergodic hypothesis for the normal canonical system of Eq. (1·2).[12)] The non-existence theorem of the isolating integral has been developed to derive the necessary condition of the global integrability.[13)~16)]

But in 1953 Kolmogorov proposed the concept of the local integrability.[17)] He derived the condition under which the unperturbed torus remains stable even in the perturbed system. The fundamental idea of Kolmogorov is to find out the *isomorphism* which smoothly transforms a quasi-periodic flow on a torus into another quasi-periodic one. For instance, consider the quasi-periodic flow on a 2-dimensional

torus,

$$dx/dt=1+\varepsilon u(x, y)\,,$$
$$dy/dt=\omega+\varepsilon v(x, y)\,, \tag{1·3}$$

where ε is a smallness parameter, (u, v) are periodic functions of (x, y) with the mod. 1, and assume the long time average of the flow vector (u, v) to be zero, $\bar{u}=\bar{v}=0$. The *rotation number* ω(=constant) is a global characteristics. The basic question is following: Is the system of Eq. (1·3) isomorphic to the unperturbed Weyl's flow ($\varepsilon=0$)? The answer is affirmative only if there exist constant parameters K and α such that,

$$|\omega-m/n|>K/n^{\alpha} \tag{1·4}$$

for all integers m and n. In other words, if the rotation number is an irrational far from resonance, the unperturbed torus is smoothly deformed into the perturbed one, that is called *the invariant torus*.[18),19)]

Moser (1962) and Arnold (1963) proved that the invariant tori (in the sense of Kolmogorov) exist even in the nearly integrable system of Eq. (1·2) under the same off-resonance condition,

$$|\boldsymbol{\omega}\cdot\boldsymbol{k}|>K/|\boldsymbol{k}|^{\alpha}\,, \tag{1·4$'$}$$

when the hamiltonian H_0 and the perturbation H_1 satisfy the following conditions:

$$|\partial^2 H_0/\partial p_i\partial p_j|\neq 0 \tag{1·5}$$

and

$$|H_1|<O(\|\partial^2 H_0/\partial p_i\partial p_j\|^{-\beta})\,, \tag{1·6}$$

where $\boldsymbol{\omega}=\{\boldsymbol{\omega}_j\}=\{\partial H_0/\partial p_j\}$, $\boldsymbol{k}$ is the integer vector, β a positive constant, and $\|A\|$ is the norm of the matrix A. The stability theorem of the torus mentioned here is called *the KAM theory*.[9),20)~24)]

When the off-resonance condition breaks, it is surmised that the unperturbed resonant torus is completely destroyed and chaotic motions comes to appear. Indeed, Zehnder (1973) proved in generic that the instability zone (in the sense of Mel'nikov) takes the place of the invariant tori in the resonance band in phase space.[25)] The onset mechanism of the instability zone was formulated by Mel'nikov for the first time with respect to the destruction of the separatrix, but the transition from torus to chaos accompanied with the breakup of the resonant torus has not yet been clearly understood in general from the theoretical viewpoint. Some of the early works done by computer are found in Ref. 29)~38).

After the resonant torus, whose rotation number is a rational, is demolished by the perturbation, the pairs of the elliptic and hyperbolic cycles are created in the resonance zone. This fact is known as the Poincaré-Birkhoff theorem, that is always satisfied in the systems with the twist condition.[20),26)] Then, not only the instability zone but also the new types of tori come to appear around the elliptic cycles, whose topological structures are quite different from that of the invariant tori of the

unperturbed hamiltonian H_0. The cascade of the transitions from torus to chaos is surmised to continue to the infinitesimal fine structure, since the resonant tori are everywhere densely embedded in phase space with the same cardinal number as the rationals. The sequences of such new born tori are often called *the islands of tori*, which are no longer the invariant tori of the unperturbed hamiltonian H_0. At the present time there is no rigorous result about the hierarchy of that islands of tori, but it is only surmised that the islands are distributed in phase space in a quite fractal manner, and that the phase space geometry is renormalizable in some sense under an appropriate scaling transformation (see § 1.3). It can be said that the transition regime between chaos and torus is the fractals' world.[27),28),58)~60)]

The KAM theory explained the conservation law of the invariant torus, and that the nearly integrable system is locally integrable. However, the theory does not say anything about the motions under the large perturbations. Every invariant torus, which belongs to the unperturbed hamiltonian H_0, is considered to vanish when the perturbation increases. In 1984 Mather derived the condition for the last invariant torus (so-called *the last KAM*) to disappear, and proved that the cantorian torus survives even after the last KAM is destroyed. The last KAM is the most stable invariant torus, and it conserves the topology of the unperturbed hamiltonian to the end.[39)~42)] His theorem is applicable only to the 2-dimensional case, but it is surmised that the cantorian torus may exist even in the higher dimensional systems,[50)~55)] and the diffusion process in chaotic regime is strongly affected by such special barrier in phase space.[55)~57)]

1.3. *Phase space geometry ——Scaling theoretical approach——*

There are two central approaches for the study of the dynamical system. One is the analytical method as is typically used in the theories mentioned in § 1.2. Another is the ergodic-theoretical approach which leads us to the statistical understandings of the system based on the thermodynamical formulation (see § 1.4).[43)~45)] However, those two approaches have not yet succeeded in explaining the fractal aspects of the phase space geometry as was mentioned in § 1.2. In the last decade, the third approach so-called the scaling theory has been exploited to attack such fractal geometry.[46)] The scaling theoretical approach is considered to bridge the gap between the analytical method and the ergodic-theoretical one. The scaling theory is based on the naive or phenomenological assumption that the phase space geometry is fractal or self-similar in some sense, and the technique is the same as is used in the renormalization group (RG) approach to the critical phenomena in statistical mechanics.[47)] Since Feigenbaum succeeded in 1979 to elucidate the renormalizable structure in the 2^n-period doubling cascade,[48)] the RG approach has been also successfully developed in the study of hamiltonian systems along the scenario discovered by Greene.[49)]

Here we try to picturize the phase space geometry only by the imagination. After a resonant torus breaks up, a lot of small islands of tori are created, and they are distributed in the resonant band in quite a complex manner. A very naive and phenomenological hypothesis is as follows. All the tori are arranged in a series of the lexicographical tree as is shown in Fig. 1. A torus is identified by a sequence of

letters $\{i_j\,;\ (i=0,1,2,\cdots:\ j=1,2,3,\cdots)\}$, where the i-class tori $\{i_k\,;\ (k=1,2,\cdots)\}$ are the daughters of a $(i-1)$-class torus $\{(i-1)_s\,;\ (s=1,2,\cdots)\}$. In this model the 0-class torus is a resonant torus that was destroyed by a perturbation. An essential point of this model is that only the break-up torus demolished by some resonance can create a lot of daughters. Some of that new born daughters are stable tori (marked by (○) in the figure) and others become unstable ones (marked by (×) in the figure) which create the granddaughters again. This hierarchy continues to infinitesimal resonant tori. As the result of such cascade, the phase space geometry even in a resonance band can be a very complicated one.

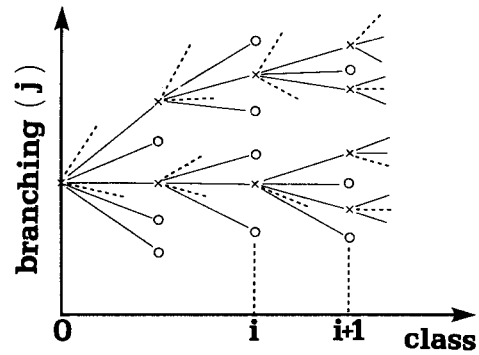

Fig. 1. A self-similarity model for the phase space geometry. The marks (○) and (×) denote the stable torus and the break-up torus respectively.

The above mentioned image is only a conjecture and may not be true in detail, but it is not altogether in the wrong. In 1983 Umberger and Farmer proposed a new concept of *fat fractals*, and numerically proved the hierarchical structure of the phase space geometry.[59] The model is much simplified by assuming that the configuration of tori is strictly self-similar.[60] Furthermore, the RG theoretical approaches elucidated that the hypothesis of the self-similarity is partially satisfied near the last KAM torus as well as the noble torus, e.g., the phase space geometry is renormalizable if one picks up from the above lexicographical tree a sub-sequence of tori whose periods can be rearranged in the Fibonaccian progression.[28),50)~55)]

The self-similarity depicted in Fig. 1 is global, and in some sense it asserts the self-similarity everywhere in the transition regime between chaos and torus.

1.4. *Characterization of chaos ——Ergodic-theoretical approach——*

A statistical behavior of the dynamical system is characterized by the time average of the dynamical quantity, e.g., $Y(x)$. The ergodic theorem asserts that there exist almost always the time average and the invariant measure $\mu(x)$ which describes it,

$$\bar{Y}\equiv\lim 1/T\int_0^T Y(x(t))dt=\int_M Y(x)\mu(dx)\equiv\langle Y\rangle\,, \tag{1·7}$$

where M denotes the whole phase space of $\{x\}$ in which the measure defined.[61),62)] The measure $\mu(x)$ is in general a function of the initial condition, and is equivalent to the asymptotic measure obtained numerically. The Birkhoff-Smith theorem states that if the space M is metrically indecomposable such invariant measure uniquely exists for almost all initial point $x(0)$ except for measure zero sets. Then the dynamical system is called metrical transitive or ergodic in the space M under that measure. As a matter of course there coexist a lot of other invariant measures in a dynamical system, but the point is that such exceptional measures are valuable only on the restricted sub-space in M. For instance, the quasi-periodic motions discussed

in § 1.2 are ergodic on the torus, though there exist other exceptional invariant measures defined on the singular set, e.g., the atomic measure restricted on a periodic orbit. But when the torus breaks up by the perturbation as is shown in the KAM theory, the measures restricted on the resonant torus disappear and new types of measures, that describe the motions on the islands' tori and/or in the instability zone, come to bifurcate. That is to say, even in the case of the nearly integrable system of Eq. (1·2) the ergodic measure is not determined uniquely, and a lot of ergodic components are heterogeneously mixed in whole space. A remarkable effect of such multi-ergodicity is discussed in § 7.

The statistical behavior of a single ergodic component E is roughly described by an ergodic measure μ_E, but the more details must be characterized by the measure theoretical structure among many ergodic sub-dynamics embedded in the singular set $E\{\rho\}$ $(\subset E)$, where measures $\mu_E\{\rho\}$'s defined in $E\{\rho\}$ are singular continuous in contrast to the dominant ergodic measure μ_E. Here ρ indicates an ergodic sub-dynamics included in E.

The characterization of chaos has been pursued in the framework of the ergodic theory.[19),21),63)~65)] A characteristics is the Lyapunov exponents which denote the time average of the orbital unfolding rates for various foliations. In the strong ergodic case such as the C-system where the unstable and stable foliations exist everywhere in phase space, the sum of the positive Lyapunov exponents is a bound of the Kolmogorov-Sinai entropy which is a well-known characteristics of the ergodic motion,[66),67),7),8)] and then the system reveals a kind of irreversibility so-called mixing. But general hamiltonian systems are not endowed with such strong condition, and that the existence of the generator which leads us to the Kolmogorov partition has not yet been proved. Therefore, the definition of "chaos" in hamiltonian systems is still unclear in the ergodic theoretical framework, but the following definition is tentatively adopted; "chaos" is the weak C-system, i.e., almost every orbit has at least one positive Lyapunov exponent. By this definition, the quasi-periodic motion on a simple torus such as the Weyl flow can be separated definitely from "chaos", since the torus motion has no positive Lyapunov exponents. But on the other hand, the instability zone (discussed in § 1.2) is very ambiguous, and is only surmised to be chaos from the computer calculations. The situation in the transition regime between "chaos" and torus is much more difficult to characterize. For instance, is the motion restricted on the critical torus such as the last KAM chaos or not?

The above definition of "chaos" seems to be useless in order to understand such critical regime. Indeed, there are many dynamical systems which generate a quite complicated behavior but whose entropy (or Lyapunov exponent) is zero. Then the sequence entropy (so-called the A-entropy) plays an inevitable role.[21),65)]

An important point of the ergodic theory is to prove the unique existence of the long time average as is shown in Eq. (1·7). But another important problem is to characterize the convergent speed toward the average value. The latter is the extension of the law of the large number, i.e., *the large deviation theory*.[68),69),117)] Such characterization of chaos is especially important for the hamiltonian flow in the transition regime between chaos and torus, because the convergent speed becomes very slow in that region and the distribution of the statistical quantity seems not to

obey the normal exponential convergence. This situation is quite analogous to the critical slowing down or the creation of the long range order near the critical point of the phase transition.

The rate of the exponential convergence is the entropy which is converted into the free energy by use of the Fenchel-Legendre transformation. The orthodox technique is the same as is used in the thermodynamical formalism in statistical mechanics.[43] But in the transition regime between chaos and torus the normal thermodynamical description is violated by the occurrence of the wild long time tails owing to the non-stationarity and the multi-ergodicity (see § 7).

1.5. *Phase space kinetics ——Non-equilibrium phenomena——*

In the transition regime between chaos and torus the essentially new concept is the *perpetual stability*, and the typical phenomenon is the occurrence of the long time tails. The first evidence was found by Nekhoroshev in 1977.[70] He succeeded in estimating the time scale for which the orbit is confined inside a certain narrow band in phase space (see § 2.1). The orbital confinement due to the perpetual stability is just the converse phenomenon to the Arnold diffusion that is induced by the topological instability. An origin of the long time tails in hamiltonian systems is in the Nekhoroshev confinement.[71),72]

The Nekhoroshev theorem enables us for the first time to study the kinetic process (or the essentially non-equilibrium process) originated from the chaotic dynamics.[80)~82] Before Nekhoroshev many works on chaos were mainly focused to the equilibrium aspects concerning the recurrence motions, though a few irreversible features such as the mixing property were studied so far. Now we are able to derive from his theorem a kinetic picture of the Arnold diffusion beyond the geometrical picture such as the "whiskered tori".[21]

An essential feature of the diffusion process (including the Arnold diffusion) is the appearance of long time tails or the enhancement of the diffusion mode with the zero frequency, e.g., the power spectral density (PSD) function $S(f)$ satisfies,

$$S(f) \sim f^{-\nu}, \qquad (f \ll 1) \tag{1·8}$$

where f stands for the frequency and ν a positive constant ($\nu > 1$).[92)~99),102)~105] Such anomalous enhancement of the zero-frequency mode cannot be observed in the integrable system of Eq. (1·1), since almost every motion is the torus with quasi-periodicity whose characteristic time scales are finite. The situation is the same for the strong ergodic system such as the K-system with a positive entropy, where the exponential decay of the correlation function can be derived from the Markov partition and such enhancement is not observed. Therefore, the singularity such as Eq. (1·8) is expected only in the transition regime between chaos and torus (or between the probability and the deterministics).

The typical one of the kinetic phenomena related to chaos is observed in the mixing process of the normal mode energy. In 1953 Fermi, Pasta and Ulam studied the problems of the kinetic process in the lattice vibration, which is a simple dynamical model of crystals.[73] They expected that the equi-partition law of the normal mode's energy will be realized after a long time. But what they obtained from the

numerical calculations was the quasi-periodic recurrence phenomena,[79] and the energy mixing was not observed. After their works many simulations have been done to confirm the existence of the unique thermal equilibrium state,[74)~78)] and the induction phenomenon which leads to the energy mixing was finally discovered by Saito and Hirooka, i.e., the energy mixing occurs remarkably after a long induction period.

In this paper we will propose a reasonable interpretation of the induction phenomena in terms of the Nekhoroshev confinement mentioned above, and that the kinetic process is considered to be a dynamical transition from torus to chaos.

1.6. *Chaos beyond ergodicity*

Chaos and torus are the dominant structures in the compact hamiltonian dynamics where the ergodic theory presupposes the Poincaré-Hopf recurrence theorem. But slow motions in hamiltonian systems (including the Arnold diffusion) are no longer the recurrent phenomenon provided that Eq. (1·8) is satisfied. The complexity of dynamical systems seems to be classified into two categories; one is the recurrent class (in the sense of Poincaré-Hopf) and another is the non-recurrent. The old ergodic theory mainly focuses onto the former, but the Arnold diffusion is beyond the recurrent class. In the present paper we will show that the hamiltonian chaos generically belongs to the non-recurrent class with the compact phase space.

Even the hamiltonian systems with the unbounded phase space can reveal not only the torus motions but also a quite complex phase. In some sense, the complexity in such systems comes from the phase shift sensitivity on the cross section in the scattering processes.[83] For an instance, the model system treated in § 4 is an example for such unbounded dynamics, and the orbit diverges to infinity as $t \to \pm\infty$. (The non-recurrent aspects of the model is not precisely discussed in this paper.) The critical phenomena between chaos and torus is expected to play an important role even in understanding the "chaos" in such scattering processes.

§ 2. Stagnant motions and the final KAM torus

In this section we will explain the basic mechanism of stagnant phenomena in hamiltonian systems, and then quickly review some useful concepts based on the 2-dimensional picture which will be used in the latter section.

2.1. *Perpetual stability and Nekhoroshev theorem*

Let us consider the nearly integrable hamiltonian,

$$H = H_0(p) + \varepsilon H_1(p, q)\,, \tag{2·1}$$

where ε is a small parameter and H is analytic. One of the fundamental problems is the following; how long does an orbit stay in the neighborhood of the unperturbed torus? When the distance in the action space $|p(t)-p(0)|$ satisfies,

$$|p(t)-p(0)| < \alpha(\varepsilon) \tag{2·2}$$

for all $t(>0)$ with a certain parameter $\alpha(\varepsilon)$ which yields $\mathrm{limit}_{\varepsilon\to 0}\alpha(\varepsilon)=0$, the orbit is

called perpetually stable.

The KAM torus discussed in § 1 is an example of such perpetually stable orbits. But in general, the perpetual stability is violated when the unperturbed torus is destroyed and is changed into a resonance zone under small perturbation. Then Eq. (2·2) should hold only for finite duration $t<T(\varepsilon)$. The Nekhoroshev theorem states,[70]

$$T(\varepsilon)\sim 1/\varepsilon\exp[1/\varepsilon^b] \tag{2·3}$$

provided $a(\varepsilon)=\varepsilon^a$, and that the constant parameters a and b do not depend on the perturbation $H_1(p, q)$ but are determined only by the unperturbed hamiltonian $H_0(p)$. The singularity factor $\exp[1/\varepsilon^b]$ plays an essential role in understanding the onset of the slow motions such as the Arnold diffusion. Equation (2·2) defines the stagnant region in the phase space where the motion is quite inactive. (The definition of the stagnant layer will be given later.)

The essential condition for the Nekhoroshev estimation is the steepness of the hamiltonian $H_0(p)$. Namely, let n be the degrees of freedom of our system and consider the n-dimensional space $\boldsymbol{p}=(p_1, p_2, \cdots, p_n)$. Denoting the lower bound of the gradient $(\nabla H_{0|s})$ in the s-dimensional sub-space λ_s by $m_{p,s}(\eta)$, i.e.,

$$m_{p,s}(\eta)=\inf_{\substack{|p-p'|=\eta \\ p'\in\lambda_s}}|\nabla H_{0|s}|\,, \tag{2·4}$$

the hamiltonian H_0 is called the steep at p if the upper bound of $m_{p,s}(\eta)$ satisfies,

$$\sup_{0<\eta<\xi} m_{p,s}(\eta)>O(\xi^{\alpha_s}) \tag{2·5}$$

with $\alpha_s>1$ (for $s=1, 2, \cdots, n-1$). The values of indices a and b are determined by α_s $(s=1, 2, \cdots, n-1)$, i.e.,

$$\begin{aligned} a&=a(\{\alpha_j\}, n)\,, \\ b&=b(\{\alpha_j\}, n)\,. \end{aligned} \tag{2·6}$$

For example, the Toda lattice hamiltonian,[84]

$$H_0(P, Q)=\sum_i\{P_i^2/2+(A/B)\exp[-B(Q_{i+1}-Q_i)]+A(Q_{i+1}-Q_i)\} \tag{2·7}$$

is rewritten by a certain transformation into,

$$H_0(p)=2\sum p_i^2\,. \tag{2·8}$$

Then the steepness index is easily derived as

$$\alpha_s=1 \tag{2·9}$$

for all s, and the indices a and b are

$$a=b=3/(6n^2-3n+14)\longrightarrow 0\,. \qquad (n\to\infty) \tag{2·10}$$

The essential singularity factor $\exp[1/\varepsilon^b]$ becomes unity as n goes to infinity and then the slow motion leading to the Arnold diffusion seems to be discarded in high dimensional systems. But as is shown later this conjecture is not true, that is to say,

the long time behaviors should not be understood without taking account of the non-stationarity owing to the stagnant effect in the perpetual stability region. The perpetual stability is locally defined in the very narrow band in phase space, but the idea is essentially important even in understanding the global wandering motions such as the Arnold diffusion.[119]

The Nekhoroshev theorem was derived for flow systems, but in this paper we assume that the theorem is applicable even for the system defined by the discrete mapping provided the motion is area preserving. The mapping in $2(n-1)$ dimensional space can be identified with the Poincaré map of a certain hamiltonian flow with n degrees of freedom.

2.2. *Scaling theoretical approach——Stagnant layer and the final KAM surface——*

Every KAM island floating in the stochastic (or chaotic) sea is always adjacent to chaotic orbits. When the dynamical system is smooth or analytic, the chaotic flow in the vicinity of a KAM surface is almost the same as the quasi-periodic motion restricted on the KAM torus because of the continuity of the flow vector. We call such local flow adjacent to a KAM surface *the stagnant motion,* and the sub-space occupied by the stagnant motions *the stagnant layer.* Furthermore, we define *the final KAM surface* as the boundary surface in which all the stagnant motions are enwrapped. Then the final KAM surface is a closed set in phase space. The final KAM may be a smooth invariant torus, but strictly speaking we cannot omit the possibility that the surface is a wild one such as the cantor set, and that the metrical transitivity might be lost on that surface. But in this paper we assume that the final KAM surface is an invariant torus with the same sense as is used in the KAM theory.

The universality of the stagnant layer can be derived from the scaling theoretical approach.[85] Let us define the stagnant layer coordinate $\boldsymbol{r}$ which denotes the distance ($n-1$ dimensional vector) from the final KAM surface as is illustrated in Fig. 2-1. Following the Nekhoroshev theorem we introduce a smallness parameter ε, i.e.,

$$r=|\boldsymbol{r}|\sim O(\varepsilon^{a}), \tag{2·11}$$

then the volume element in the $\boldsymbol{r}$-space is

$$d\boldsymbol{r}\sim O(\varepsilon^{a'-1})d\varepsilon, \tag{2·12}$$

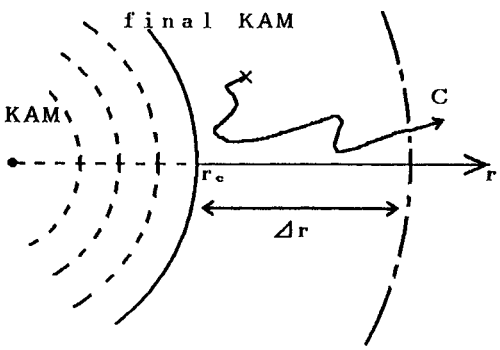

Fig. 2-1. The stagnant layer coordinate. Δr denotes the phenomenological threshold for the stagnant motion.

where $a'=a(n-1)$. The phase volume V of the stagnant layer (i.e., Lebesgue measure of the r-neighborhood) is a function of $\boldsymbol{r}$ and the phase volume element dV satisfies,

$$dV\sim P(\boldsymbol{r})d\boldsymbol{r}, \tag{2·13}$$

where $P(\boldsymbol{r})$ is the invariant density. As the density has no singularity, the pausing time distribution $P(T)$ is derived,

$$P(T)\sim|dV/dT|\sim\varepsilon^{a'-1}|d\varepsilon/dT|$$

$$\sim\frac{1}{T}\left(\frac{1}{\log T}\right)^{1+a'/b}, \tag{2·14}$$

where we used Eq. (2·3) in the limit of $\varepsilon\to 0$,

$$\begin{aligned} &|d\varepsilon/dT|\sim\varepsilon^{2+b}\exp[-1/\varepsilon^b]\,,\\ &\log T\sim\varepsilon^{-b}\,. \end{aligned} \tag{2·3$'$}$$

When the initial points are uniformly distributed in the stagnant layer $r<\Delta r$ (see Fig. 2-1), the distribution $P(T')$ for the first passage time T' necessary for the representative orbit C to escape from the threshold level is given by $dr/\Delta r$, i.e.,

$$P(T')\sim\frac{1}{T'\log T'}\,. \tag{2·15}$$

This is a universal law in the stagnant layer.

Equation (2·11) reveals the meaning of the smallness parameter ε, i.e., in the above discussion the basic assumption is that the unperturbed motion is the final KAM torus and the distance $\boldsymbol{r}$ is the effective perturbation to it. This is compatible with the previous assumption such that the final KAM surface is an invariant torus.

Next let us consider the inside of the final KAM surface, i.e., the stable region for $\boldsymbol{r}<0$ in Fig. 2-1. In the stable region we assume that almost whole space is densely covered with invariant tori. This is not generally correct in high dimensional systems, but is approximately correct in two dimensional systems (see § 5). When we consider the distance r as a control parameter, a kind of phase transition seems to occur at the critical value of $r=r_c$ $(=0)$. Then the final KAM surface corresponds to the critical point at which the stable phase takes the place of the chaotic one.

In the system with 2 degrees of freedom, the rotation number of the invariant torus $R(p)$ is the best candidate for the order parameter to describe the phase transition, where p is the action variable. Denoting the angular frequency by R $(=\omega_1/\omega_2)$, the order parameter is given by the long time average of it. The derivative dR/dp stands for the relative shear stress of the circulating flow along the KAM surface, since ω is the gradient of the hamiltonian,

$$\omega_j=\partial H_0/\partial p_j\,. \tag{2·16}$$

Our basic assumption is formulated as follows; under an appropriate canonical transformation, the original system of Eq. (2·1) can be rewritten into,

$$H'(r,\theta)=H_0'(r,\varepsilon)+H_1'(r,\theta,\varepsilon)\,, \tag{2·17}$$

where the variable θ is the canonical conjugate to the new action variable r. The point is that the renormalized perturbation H_1' is effectively zero for $r<r_c(=0)$. Therefore, the order parameter $R(r)$ is

$$R(r)=\lim_{T\to\infty}1/(2\pi T)\int_0^T\partial H_0'/\partial r dt \tag{2·18}$$

for all $r(<r_c)$. As was proved by Arnold,[9] the necessary condition for the invariant torus to survive under the perturbation H_1' is,

$$|H_1'| < A_n \Theta^{-c}, \tag{2·19}$$

where A_n is a function of the degree of freedom n, and c is a positive constant, and Θ is the upper bound of the local shear stress, i.e.,

$$\Theta = \max\|\partial^2 H_0'/\partial r^2\| \sim O(dR/dr). \tag{2·20}$$

Therefore, if the final KAM is the critical invariant torus that becomes unstable under every infinitesimal perturbation, the gradient dR/dr must be infinity at $r=r_c$. This implies that the order parameter $R(r)$ should be singular as is shown in Fig. 2-2, for instance,

$$R(r) \sim (r_c - r)^{\alpha}, \qquad (\alpha < 1) \tag{2·21}$$

for $r_c > r$, and $R(r)=\text{const}$ for $r_c < r$.

In § 5 we will numerically pursue the critical phenomena near the final KAM surface. The results seem to support the existence of the phase transition, though our approach is based on the phenomenological assumption mentioned above.

2.3. *Statistical laws in a stagnant layer*

Here we give some heuristic comments on the general aspects in the stagnant layer. The mean values of the first passage time as well as the pausing time become infinity owing to Eqs. (2·14) and (2·15). This enables us to define the pure stagnant motions, that is to say, the motions which are perpetually trapped in the stagnant layer. The invariant measure that describes such motions is different from the Lebesgue measure of Eq. (2·13), and is surmised to be strongly localized around the final KAM surface. As will be discussed in § 6, the most dominant one of such measures $P(r)$ is expressed by

$$P(r) \sim r^{-\alpha}, \qquad (r > 0) \tag{2·22}$$

where r stands for the distance from the final KAM surface (i.e., $r_c=0$) and α a positive constant. If the rate of the orbital unfolding λ is a function of r, i.e.,

$$\lambda \sim r^{d} \tag{2·23}$$

with a positive constant d, the distribution of λ becomes,

$$P(\lambda) \sim \lambda^{-\delta} \tag{2·24}$$

with $\delta = 1 + (\alpha - 1)/d$. Intuitively, λ is the local Lyapunov exponent in the stagnant layer, and the first passage time T' is estimated by $T'\lambda \sim 1$ and the distribution of the first passage time $P(T')$ becomes,

$$P(T') \sim T'^{-\beta}, \quad (\beta = 2 - \delta) \tag{2·25}$$

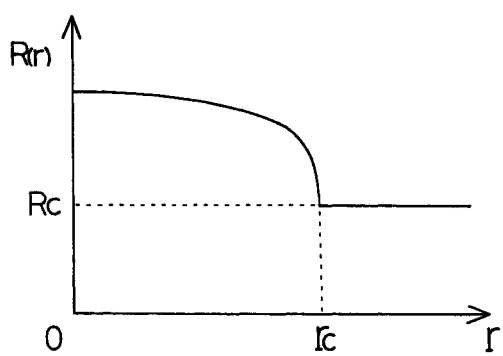

Fig. 2-2. The change of the rotation number $R(r)$. r stands for the stagnant layer coordinate.

where $\delta=1$ (or $\alpha=1$) is predicted in line with Eq. (2·15).

The essence of the pure stagnant motions is the non-stationarity; the characteristic time scale dt and the spatial scale dr satisfy the following relation:

$$dt/dr \sim 1/\lambda r \sim O(r^{-d-1}) . \tag{2·26}$$

This implies that any orbits cannot reach to the final KAM surface in a finite time,

$$\int dt \sim \int_{r_0}^{0} r^{-d-1} dr \longrightarrow \infty , \tag{2·27}$$

where r_0 stands for the initial position.

When we introduce the new coordinate Y, i.e., $dY/dr=-r^{-d-1}$, Eq. (2·26) is rewritten into

$$dY/dt=\eta(t)$$

or

$$Y(t) \sim \int^{t} \eta(t')dt' . \tag{2·28}$$

Here the non-singular part $\eta(t)$ of Eq. (2·26) is introduced. We can assume that $\eta(t)$ is originated from the chaotic behavior in the stagnant layer and is a stationary variation. For an instance, when $\eta(t)$ is a white gaussian process, $Y(t)$ becomes the Wiener process (or the Brownian motion). If the approximation is correct in the large time scale limit, the power spectral density (PSD) of the variable $Y(t)$, i.e., $S(f;\ Y)$ becomes

$$S(f;\ Y) \sim f^{-2} \tag{2·29}$$

in the low frequency limit ($f \ll 1$). The non-stationarity of Eq. (2·29) will be discussed in § 4 by putting $d=0$, i.e., $Y=-\log(r-r_c)$.

The fluctuation of the phase angle $\theta(t)$, which is the canonical conjugate to the radial coordinate $r(t)$, is obtained from the same consideration. Let us denote the characteristic frequency of the final KAM torus by f_c. Then the rotation velocity $d\theta/dt(=2\pi f)$ at the distance r ($>r_0$) satisfies,

$$\begin{aligned} 2\pi(f-f_c) &= \dot{\theta}(t)-\dot{\theta}_0(t) \equiv \Delta\dot{\theta}(t) \\ &\sim O(r^{d}) \end{aligned} \tag{2·30}$$

since the system is the area preserving one. Here $\theta_0(t)$ denotes the phase angle on the final KAM torus. Therefore, the distribution of the frequency $P(f)$ obeys the same scaling form as stated in Eq. (2·24),

$$P(f) \sim |f-f_c|^{-\delta} . \tag{2·31}$$

Furthermore, the PSD of the fluctuating period $\tau(=dt/d(\theta-\theta_0) \sim O(r^{-d}))$ is the same as that of $Y(t)$ in Eq. (2·28),

$$S(f;\tau)\sim f^{-2}. \qquad (f\ll 1) \tag{2·32}$$

Equations (2·31) and (2·32) explain the general aspect of the phase noise in hamiltonian systems.[88] If the stationary process $\eta(t)$ is submitted to the fractional Brownian motion $B_H(t)$, i.e.,

$$B_H(t)=\int^t (t-s)^{H-1/2}dB(s) \tag{2·33}$$

and

$$\eta(t)dt=dB_H(t), \tag{2·34}$$

the phase noise should be generalized as,

$$S(f;\tau)\sim f^{-(2H+1)}, \qquad (f\ll 1) \tag{2·35}$$

where $B(t)$ stands for the Wiener process and H a parameter $(0<H<1)$.[86),87)]

2.4. *Large scale diffusion ——Symbolic dynamical realization——*

In general, innumerable KAM islands are distributed in phase space, and as the result the stagnant layers without number are also coexisting. Denoting the size (or the phase volume) of an island by v, the distribution of the size $P(v)$ seems to satisfy,

$$P(v)\sim v^{D'-1}, \tag{2·36}$$

where D' (<1) is a positive constant (see § 6). Besides, the geometrical disposition of each KAM island is surmised to be self-similar as is shown in Fig. 2-3. Such self-similar structure is called *the fat fractals*.[59]

The fat fractal structure induces a new universal aspect in the long time tails of hamiltonian systems. Let us denote the i-th stagnant layer by L_i, and consider the jump process from L_i to L_j. The pausing time in each stagnant layer is extremely long, but on the other hand the residence time in the non-stagnant layer $\tilde{L}$ (=the compliment of the set $\bigcup_k L_k$) is rather short. Therefore, the long time behavior of the system can be characterized by the reduced dynamics ϕ in the symbolic space $\{L_1, L_2, L_3, \cdots\}$, i.e., ϕ: $L_{i_1}\to L_{i_2}$. The merit of the symbolic dynamical approach is that the mapping is well approximated by a semi-markoffian process as was discussed in the previous paper;[89)~91)] the PSD of the symbolic process $\{i_1\to i_2\to i_3\to,\cdots\}$, i.e., $S(f;i)$, reveals the long time tail,

$$S(f;i)\sim f^{-(3-\beta)}, \qquad (f\ll 1) \tag{2·37}$$

when the pausing time distribution $P(T)$ in each symbolic state satisfies,

$$P(T)\sim T^{-\beta}. \qquad (T\gg 1) \tag{2·38}$$

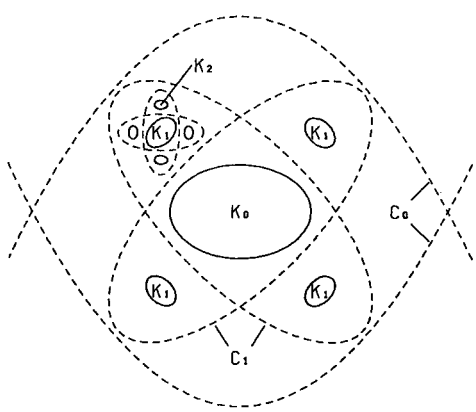

Fig. 2-3. A fat fractal picture of "islands around islands". Circles denote the final KAM surfaces. The C_i's denote the ghost separatrices.

Equation (2·37) suggests a universal aspect ($\beta=1$ from Eq. (2·15)) of the Arnold diffusion in the symbolic space. As the PSD is not invariant under the general isomorphic translation, we cannot always observe the f^{-2} spectrum for a given variable. But the point is that the non-stationary diffusion process is almost always hidden behind the fat fractal structure.

§ 3. Numerical proof of the stagnant motion

In this section we will give a direct evidence of the Nekhroshev theorem carrying out with computer simulations. The model system is the billiard motion in the generalized stadium.[101]

The boundary of the stadium is constructed by four convex arcs as is shown in Fig. 3-1. First, fix a square $ABCD$ (e.g., $AB=2$) and draw the circular arcs (AD and BC) with the same radius a, and then the remaining arcs (AB and CD) are drawn as their derivatives are continuous at each end point. In this model let the system parameter be $\delta=\sqrt{a^2-1}$. At $\delta=0$ the system becomes the Bunimovich stadium where the motion is completely ergodic (i.e., K-system), and the case $\delta=1$ is completely integrable.[100]

The Birkhoff coordinates (i.e., the normalized arc length η $(0<\eta<1)$ and the reflection angle-coordinate $s=\sin\alpha$ in Fig. 3-1) are used to describe the motion of the billiard ball.[26] A collision point (η_i, s_i) is successively transferred to the next collision point (η_{i+1}, s_{i+1}) due to the area-preserving mapping T_δ,

$$T_\delta:(\eta_i, s_i)\longrightarrow(\eta_{i+1}, s_{i+1})\,. \tag{3·1}$$

In this paper simulations will be limited only to the nearly ergodic case ($\delta\ll1$), where the final KAM surface is clearly observed and the analysis becomes rather easy.

Figure 3-2(a) shows the mapping for a chaotic orbit. All the KAM tori in this system are squeezed into two narrow bands which are shown as white holes in the figure. Roughly speaking, these narrow bands correspond to the perpetual stable region discussed in § 2, and the center of each band is a stable cycle with period 2. There is no KAM islands anywhere in phase space except for in these bands. Figure 3-2(b) is the magnification of a part of the stagnant layer, where a lot of KAM islands are dispersed.

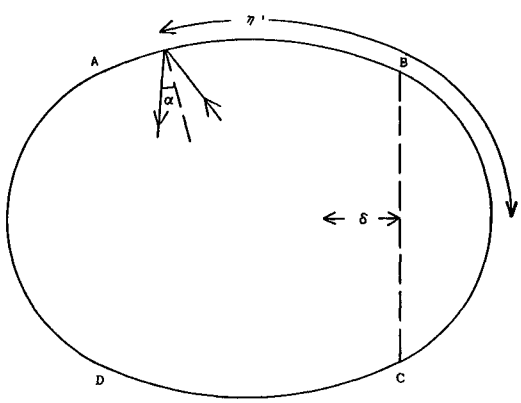

Fig. 3-1. The billiard system in the generalized stadium.

By using the fact that the final KAM surface of our case ($\delta\ll1$) is an almost complete ellipse, we introduce new coordinates (r and θ),

$$\eta-\eta_c=r\cos\theta\,,$$
$$s=1/Ar\sin\theta\,, \tag{3·2}$$

where $\eta_c(=0.25)$ is the position of the elliptic center and $A(\fallingdotseq30.752\cdots)$ is the

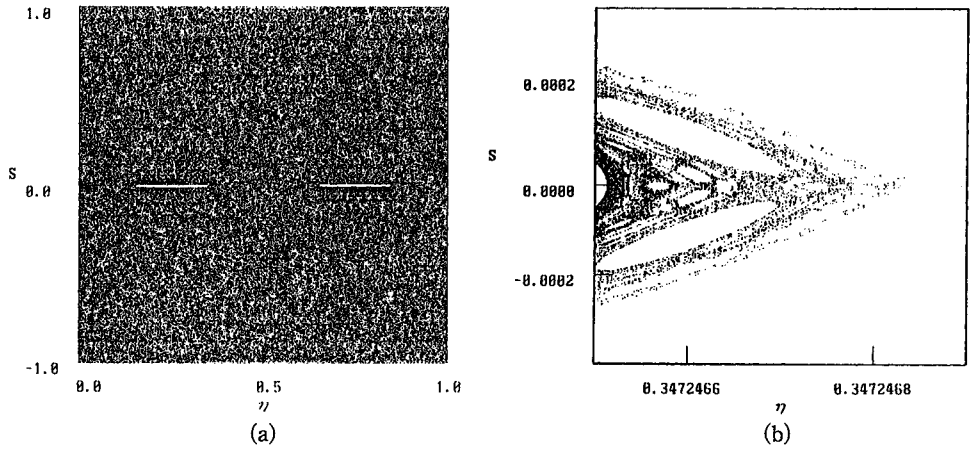

Fig. 3-2. The mapping in the normalized Birkhoff's coordinates.
(a) The mapping for the generalized billiard.
(b) The magnification of the stagnant zone observed in (a).

scaling factor. Figure 3-3 shows the magnification of the stagnant layer. The radius of the final KAM surface $r=r_c=0.0972\cdots$, and the thickness of the stagnant layer $\Delta r=10^{-6}$ approximately.

We distribute the initial ensemble uniformly in this thin layer $(r-r_c<\varepsilon)$, and estimate the first passage time T necessary for each orbit to escape from the threshold level ε. The first passage time distribution $P(T)$ is illustrated in Fig. 3-4. The exponential distribution (Fig. 3-4(a)) is realized in short time behavior for large ε. In order words, the non-stagnant motion is dominant in the region far from the final KAM surface, where the markoffian approximation is well adjustable. But in the stagnant layer very near from the final KAM the distribution obeys the non-markoffian hyperbolic one for large T,

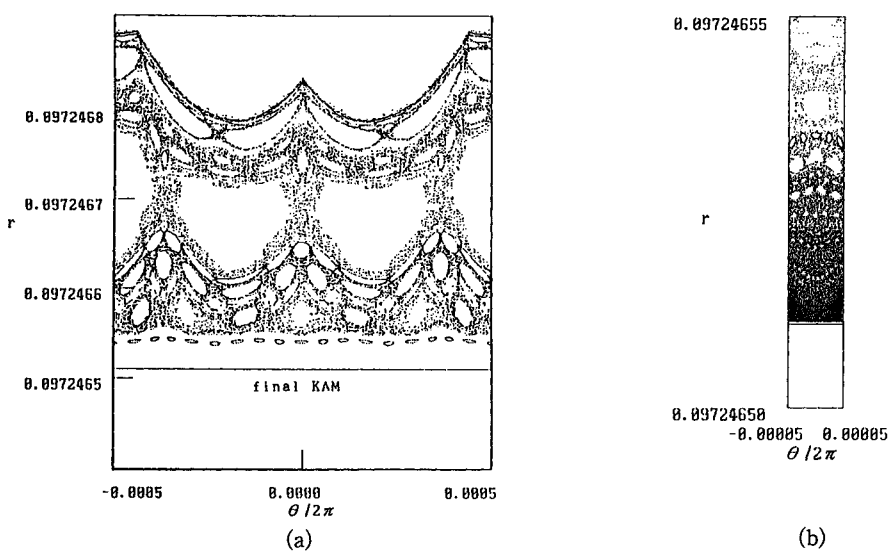

Fig. 3-3. (a), (b) The stagnant layer magnified in the (r, θ) space.

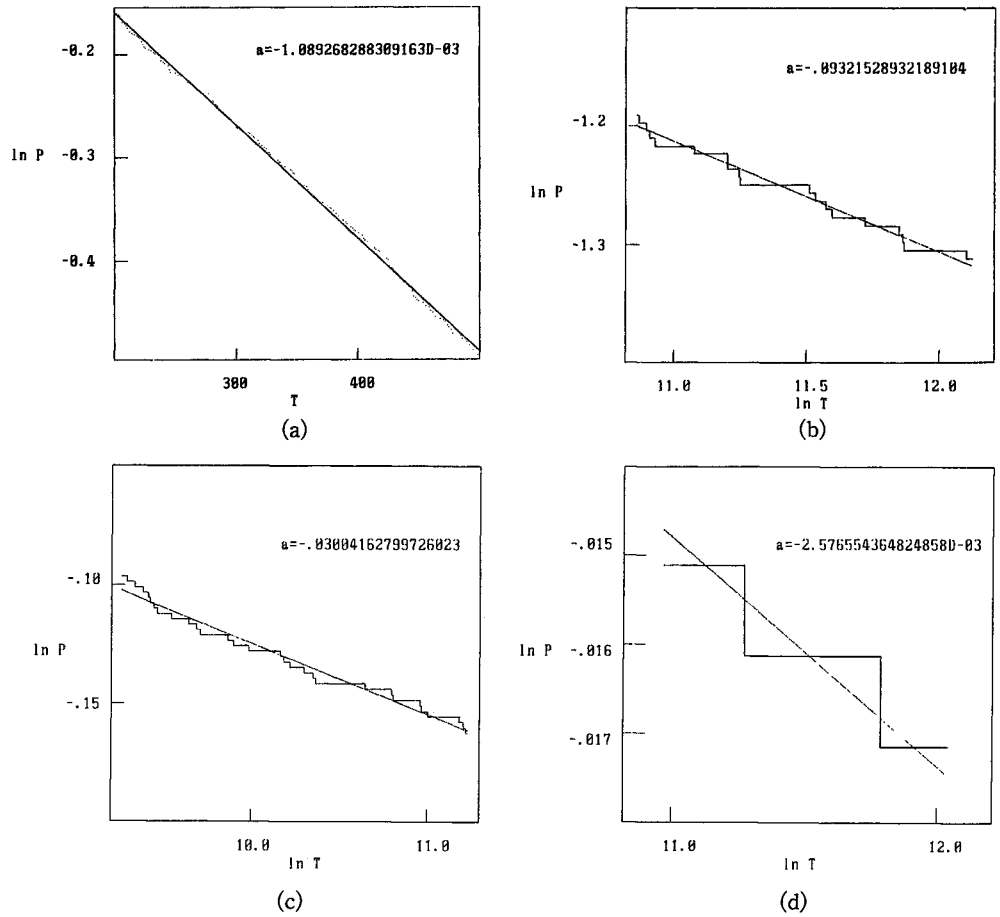

Fig. 3-4. The first passage time distributions $P(T)\sim T^{-\beta}$ $(a=1-\beta)$.
(a) For $\varepsilon=2\times10^{-6}$ (exponential decay: $P(T)\sim\exp[aT]$ with $a=-0.000109$).
(b) For $\varepsilon=5\times10^{-7}$, $a=-0.093215$.
(c) For $\varepsilon=3\times10^{-7}$, $a=-0.030041$.
(d) For $\varepsilon=10^{-7}$, $a=-0.002576$.

$$P(T)\sim T^{-\beta} \tag{3·3}$$

and the index $\beta(\varepsilon)$ seems to decrease,

$$\beta(\varepsilon)\to 1, \qquad (\varepsilon\to 0) \tag{3·4}$$

in accordance with Eq. (2·15). In the numerical analysis the time domain is nearly fixed as $10^{10}<T<10^{12}$ in line with the precision of the machine calculation, and the integrated distribution function was used in Fig. 3-4.

The time course of one sample path in the stagnant layer is shown in Fig. 3-5. The distance from the final KAM surface increases almost monotonically for short time, and intermittently it reveals sharp enhancement. Especially big jumps are observed near $r-r_c\sim10^{-7}$. Such anomalous enhancement may come from the diffusion barrier due to the cantorus or the heteroclinic narrow gates in phase space. The long time tails of Eq. (3·3) might be correlated to such special structure in phase

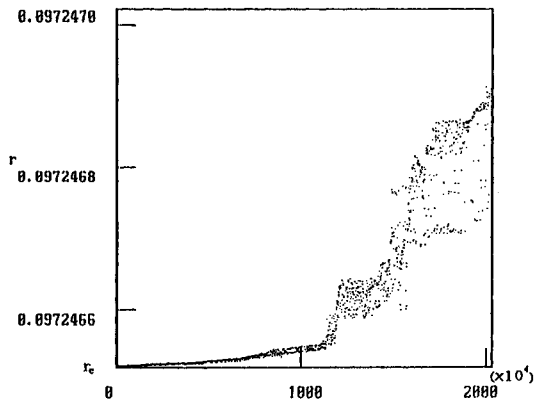

Fig. 3-5. A diffusion process of one sample path.

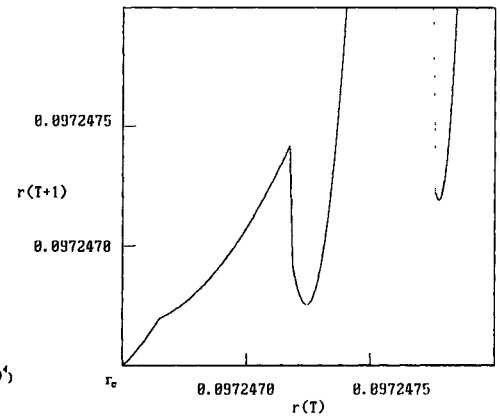

Fig. 3-6. One dimensional realization of the stagnant motion. r_c denotes the coordinate of the final KAM surface.

space.

The essence of the stagnant layer can be extracted in a one-dimensional reduced mapping. We consider the narrow strip which satisfies $|\theta-\pi/2|<10^{-5}$ in phase space (r, θ). When an orbit reinjects into the strip successively at time $t_1, t_2, \cdots$, denote the radial coordinate by $\{r_1, r_2, r_3, \cdots\}$. Then let us consider the return mapping ϕ,

$$\phi: r_T \to r_{T+1}\,. \tag{3·5}$$

Figure 3-6 reveals a striking structure that is quite similar one as is observed in the well-known intermittent map for $|r-r_c| \ll 1$, i.e., [106)~112)]

$$r_{T+1}-r_T \propto (r_T-r_c)^B\,. \qquad (B>2) \tag{3·6}$$

This remarkable point will be discussed again in § 6.

§ 4. Induction phenomena and the Arnold diffusion

Let us consider the discrete time lattice vibration of linear chain described by the following mapping:

$$x_{n+1}^i-2x_n^i+x_{n-1}^i=K(x_n^{i+1}-2x_n^i+x_n^{i-1})+\left(\frac{N+1}{2}\right)^2\mu\{(x_n^{i+1}-x_n^i)^3+(x_n^i-x_n^{i-1})^3\}\,, \tag{4·1}$$

$$(x_n^0=x_n^{N+1}=0)$$

where the integer i stands for the lattice site and n discrete time.*) K is the linear spring constant and μ the cubic nonlinear perturbation. When $\mu=0$, by introducing the normal mode coordinate Q_n^j's, the equations of motion are rewritten into

*) The nonlinear term should be replaced by

$$\{(x_n^{i+1}-x_n^i)^3-(x_n^i-x_n^{i-1})^3\}$$

for the Fermi-Pasta-Ulam problems discussed in § 1, but the induction phenomena are not clearly observed under such perturbations.

$$Q_{n+1}^j - 2Q_n^j + Q_{n-1}^j = -\omega_j^2 Q_n^j\,, \qquad (\omega_j^2 = 4K\sin^2 j\pi/2(N+1)) \tag{4·2}$$

where the transformation is unitary,

$$x_n^i = \sqrt{2/(N+1)}\sum_{j=1}^{N} Q_n^j \sin \pi ij/(N+1)\,. \tag{4·3}$$

The constant of motion which corresponds to the energy of each normal mode E_n^j becomes,

$$E_n^j = (Q_{n+1}^j - Q_n^j)^2 + \omega_j^2 Q_{n+1}^j Q_n^j\,. \tag{4·4}$$

When we introduce the perturbation μ, E_n^j's are not invariant but fluctuating in time. Defining the canonical momentum P_n^j by

$$P_n^j = Q_{n+1}^j - Q_n^j\,, \tag{4·5}$$

the mapping ϕ: $(P^1, \cdots, P^N; Q^1, \cdots, Q^N) \circlearrowleft$ becomes a measure preserving one. The special case $N=2$ and $K=1$ is studied in what follows, namely that is the simplest model which reveals the Arnold diffusion.

Figure 4-1 shows the mapping in the normal mode space for $\mu=0$, where the orbit is two dimensional torus described by Eqs. (4·4) and (4·5). For the case $\mu \neq 0$, the Arnold diffusion occurs as is shown in Fig. 4-2. When the time t is smaller than a certain induction time T_I, the energy of each normal mode oscillates pseudo-periodically and the orbit seems to be a simple torus. But for the case $t > T_I$, the orbit becomes strongly chaotic. The switching from the pseudo-periodicity to chaos is instantaneously achieved at $t = T_I$ as is shown in Fig. 4-3. This is the induction phenomena of our system. After the transition at $t = T_I$, the exchange of the energy occurs drastically but the equi-partition law of energy has not yet been satisfied in this model.

Here we will numerically prove that the pseudo-periodic motion (for $t < T_I$) is the stagnant motion such as discussed in § 2, i.e., the induction time T_I obeys the Nekhoroshev estimation;

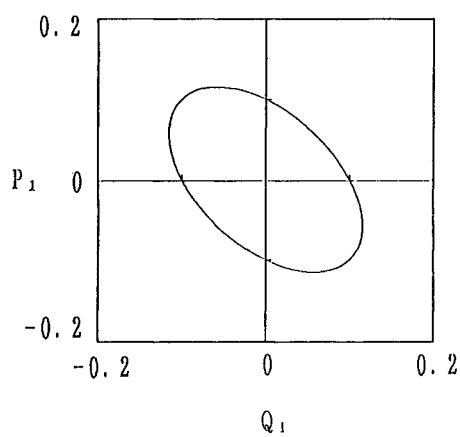

Fig. 4-1. The mapping of the first normal mode (P_1, Q_1) at $\mu=0$.

$$T_I \sim T_\mu \equiv \frac{1}{|\mu-\mu_c|}\exp[(\mu-\mu_c)^{-b}]\,, \tag{4·6}$$

and the distribution of the induction time T_μ becomes

$$P(T_\mu) \sim \frac{1}{T_\mu}\frac{1}{\log T_\mu}\,, \tag{4·7}$$

where μ_c is the adjustable value of μ at which the orbit is completely quasi-periodic under the initial condition used in the simulation. In other words, the orbit is a perpetually stable torus at $\mu = \mu_c$ and the induction phenomenon does

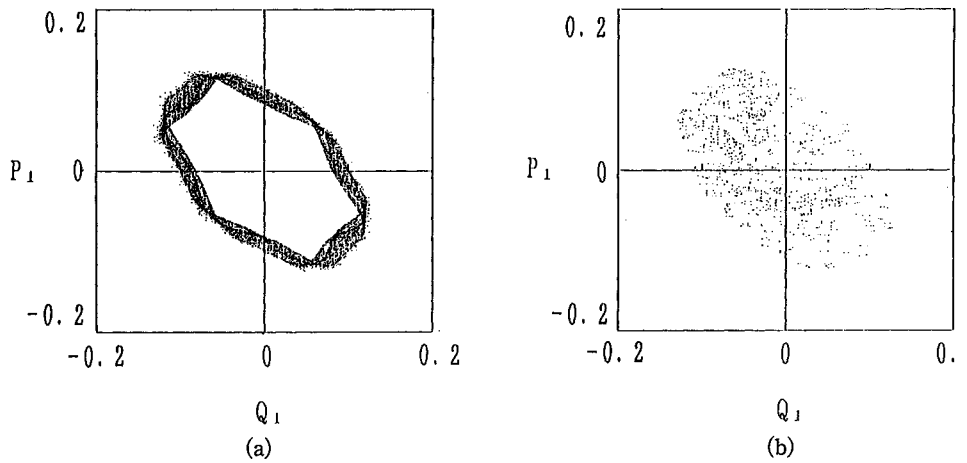

Fig. 4-2. The mapping of the normal mode (P_1, Q_1) at $\mu=21$.
(a) For $t<T_I$. (b) For $t>T_I$.

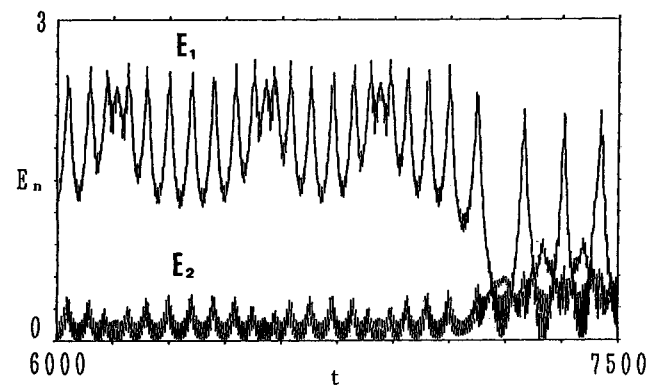

Fig. 4-3. The time course of the normal mode's energy E_1 ($\mu=9.45\times10^{-2}$). The energy mixing begins at $t\fallingdotseq T_I(\fallingdotseq 7200)$.

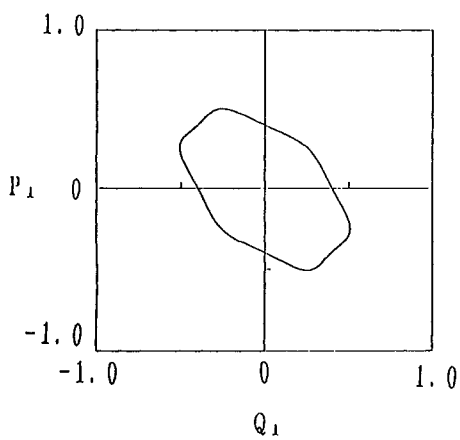

Fig. 4-4. The final KAM surface determined numerically at $\mu=0.333$ and (P_1, P_2, Q_1, Q_2) $=(0.4, 0, 0, 0)$.

not occur (see Fig. 4-4).

The induction period T_μ is measured for a fixed initial condition ($P_1=0.4$, $P_2=0$, $Q_1=0$, $Q_2=0$). As one can see in Fig. 4-5, T_μ changes step-wisely. This implies that the geometrical structure of phase space is very intricate and that the Arnold diffusion is sensitively dependent on the initial condition. If we neglect the step-wise small structure, the overall feature of Fig. 4-5 is well adjustable by Eq. (4·6) putting $\mu_c=0.333$ and $b=400$.

Next we determine the probability density of the induction period T_μ by

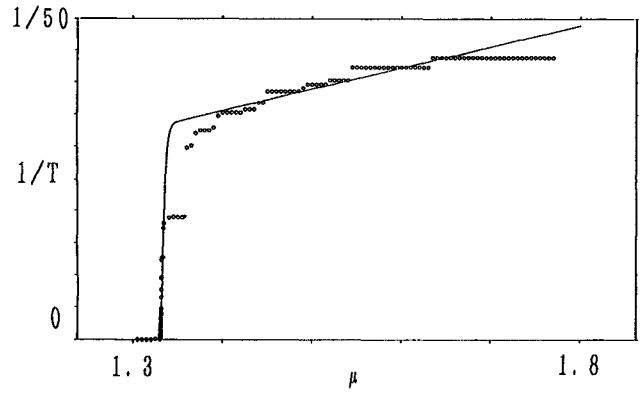

Fig. 4-5. The induction periods for various values of μ. The solid line is the Nekhoroshev bound adjusted by Eq. (4·6) with $\mu_c=0.333$ and $b=400$.

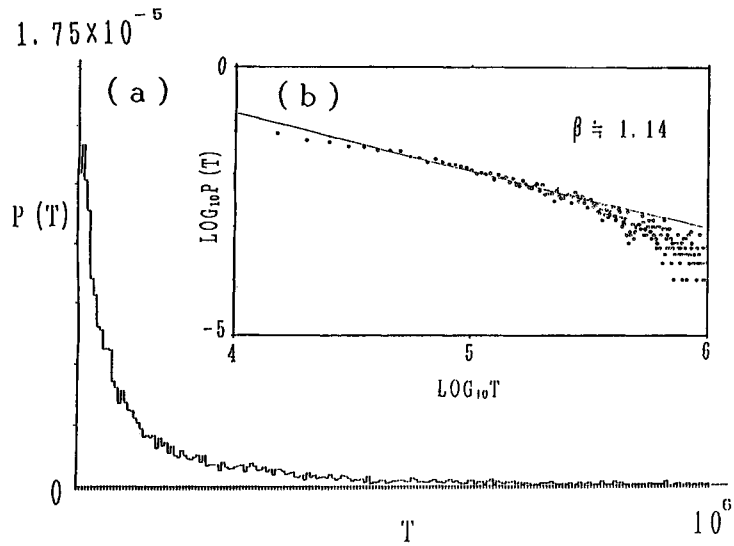

Fig. 4-6. The distribution of the induction period for the initial ensemble of the small window.
(a) Normal plot ($P(T)\sim T^{-\beta}$).
(b) Logarithmic plot: The solid line denotes the fitting by Eq. (2·15), and the ordinate is shifted by Log(5000).

fixing the value of $\mu(=21)$. In the first simulation (Fig. 4-6), the ensemble of the initial points is taken to be uniform in the small window satisfying,

$$|P_1-0.1|<3.125\times10^{-4},$$

$$|Q_1|<3.125\times10^{-4}$$

with $P_2=Q_2=0$. The second simulation (Fig. 4-7) follows to another ensemble with random phases on the torus described by Eq. (4·4) with the same initial energy as in the previous simulation. Either case seems to be adjustable by the inverse power law ($P(T)\sim T^{-\beta}$) with $\beta=1.14$ or $\beta=1.02$ respectively for large $T(\gg10^4)$. The solid lines in Figs. 4-6(b) and 4-7(b) indicate the fitting by Eq. (2·15).

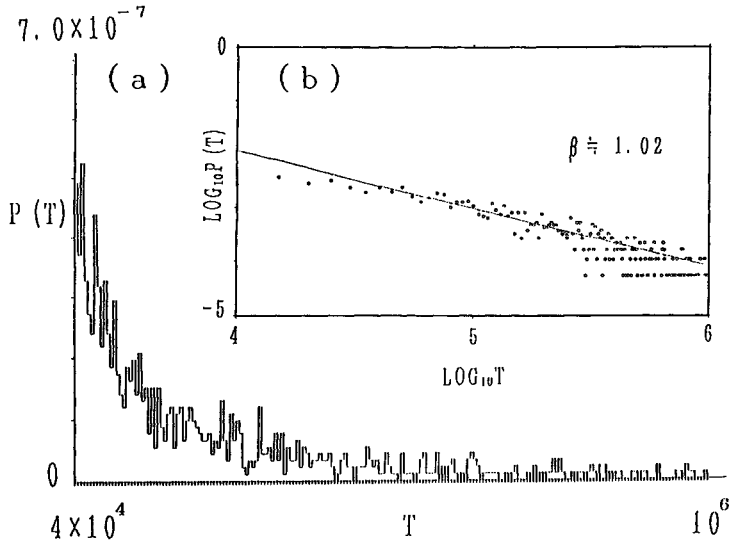

Fig. 4-7. The distribution of the induction period for the initial ensemble of the random phase.
(a) Normal plot ($P(T) \sim T^{-\beta}$).
(b) Logarithmic plot: The solid line denotes the fitting by Eq. (2·15), and the ordinate is shifted by Log(5000).

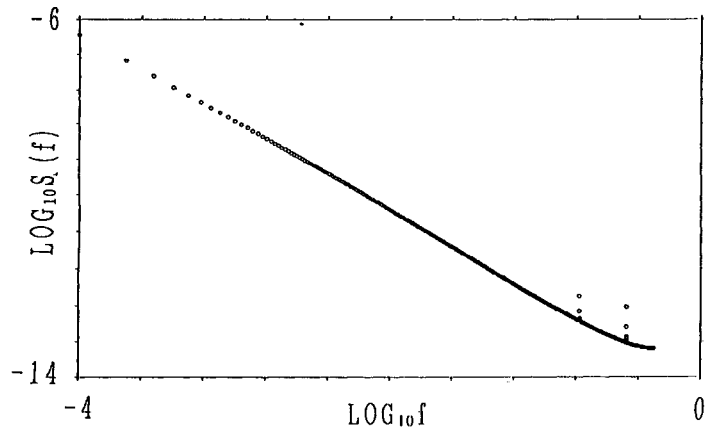

Fig. 4-8. The power spectrum of the variable $X=\log(E_1(t)/E_1(0))$ for $t<T_I$, where $\mu=10^{-3}$ and $(P_1, P_2, Q_1, Q_2)=(1, 0, 0, 0)$.

In spite of the good agreement between the induction phenomenon mentioned here and the Nekhoroshev theory, precisely speaking there still remains a big problem unsolved. Namely, there may coexist a number of stagnant layers in the neighborhood of the initial conditions used here, and the orbits may pass by them one after another before the induction occurs. If so, the induction phenomenon should not be understood in terms of the simple diffusion process in a stagnant layer, but must be understood as the compound jump process among a lot of stagnant layers as was discussed in § 2.4.

The striking aspect of the diffusion process for $t<T_I$ is revealed in the PSD function $S(f; X)$ of the new variable $X(=\ln\{E_1(t)/E_1(0)\}$, where $E_1(t)$ denotes the

energy of the first mode;

$$S(f;X)\sim f^{-2} \tag{4·8}$$

as is shown in Fig. 4-8. This is the same spectrum as for the Brownian motion, and should be understood in relation to Eqs. (2·37) and (2·38).

§ 5. Critical phenomena of the final KAM surface

In this section we will try to characterize the singularity of the final KAM torus along the same line that was discussed in § 2.2. Two-dimensional mappings are numerically studied, i.e., Hénon map, Standard map, and Tennyson map.

Hénon map[113)]

$$x'=(\cos 2\pi\alpha)x-(\sin 2\pi\alpha)(y-x^2)\,,$$

$$y'=(\sin 2\pi\alpha)x+(\cos 2\pi\alpha)(y-x^2)\,. \qquad (\alpha=0.2114) \tag{5·1}$$

The distance r denotes the x-coordinate on the symmetry line, $y=(\tan\pi\alpha)x$, as is shown in Fig. 5-1. The point of $r=0$ is the elliptic center surrounded by invariant KAM tori. The invariant surface vanishes for $r>r_c$ $(=0.405289\cdots)$, and the very narrow chaotic band appears owing to the heteroclinicity of unstable cycles with the period 5. The KAM torus at $r=r_c$ is the final KAM which will be analysed hereafter. The rotation number of the invariant torus $R(r)$ is shown in Fig. 5-2, where the initial point is put on the symmetry line with the distance r. $R(r)$ is well defined for $r<r_c$, but is fluctuating above the critical point $(r>r_c)$. The anomaly observed near the final KAM surface reminds us the scaling law in the order-disorder phase transition, e.g., in the analogy with the magnetic spin system, the order parameter R corresponds to magnetization and the control parameter r to temperature. We do not have any special reason to believe that the singularity of the final KAM surface obeys to the same scaling law as the ferromagnetic phase transition, but in what follows we will pursue the possibility of a certain universal law near the critical point $r=r_c$.

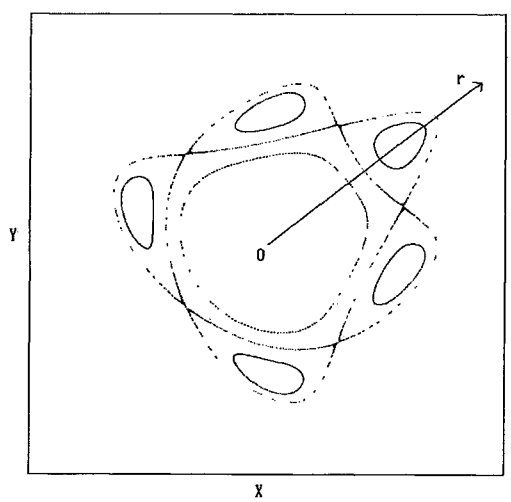

Fig. 5-1. The sketch of the Hénon mapping. The stagnant layer coordinate is measured along the r-axis in the figure.

Two scaling forms are examined,

$$\text{(A)}\quad R-R_c\propto(r_c-r)^{\alpha} \tag{5·2}$$

and

$$\text{(B)}\quad R-R_c\propto\{\ln(r_c-r)^{-1}\}^{-1/\beta}\,, \tag{5·3}$$

where $R=R(r)$ and $R_c=R(r_c)$. The second implies the essential singularity,

$$r_c-r\sim\exp\{-(R-R_c)^{-\beta}\}\,. \tag{5·3$'$}$$

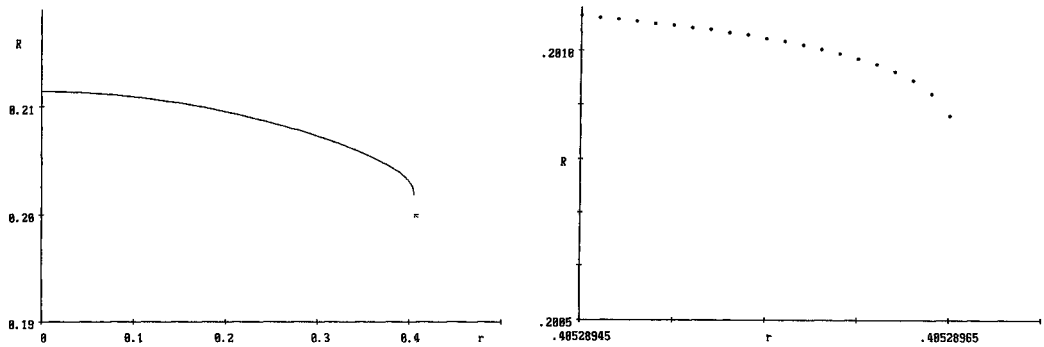

(a) (b)

Fig. 5-2. The singularity of $R(r)$ in the Hénon mapping.
(a) The numerical data of the rotation number $R(r)$ for the Hénon map.
(b) The magnification of (a) near the transition point.

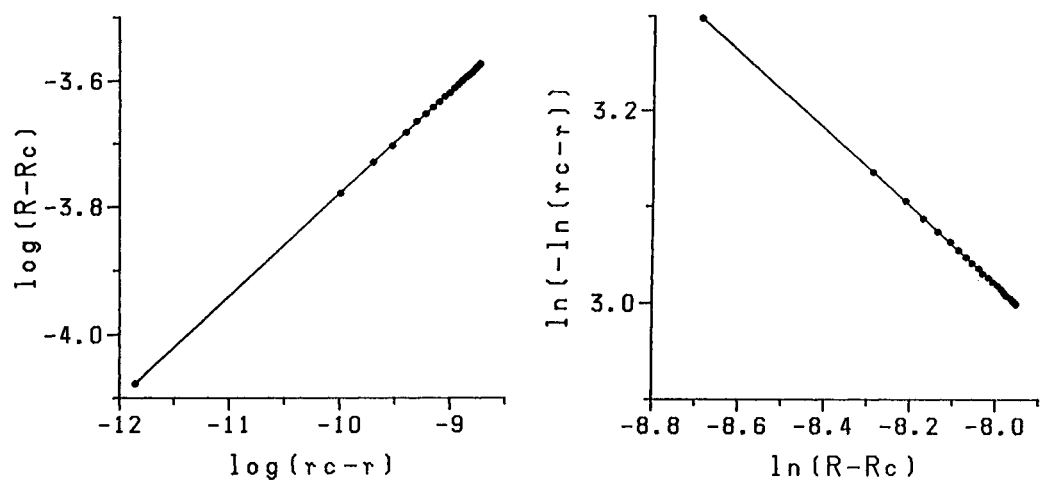

(a) (b)

Fig. 5-3. The scaling regime for the Hénon map. (a) Fitting by Eq. (5·2). (b) Fitting by Eq. (5·3).

We have used the weighted least square method to determine the critical index and the critical point (r_c, R_c), and get the most reliable values for them;

$$\text{(A)}\quad \alpha=0.117\cdots,\qquad r_c=0.40528965772811\cdots,$$
$$R_c=0.200485906\cdots,$$
$$\text{(B)}\quad \beta=0.891\cdots,\qquad r_c=0.40528965749838\cdots,$$
$$R_c=0.200125357\cdots.$$

The critical points (r_c, R_c) are almost the same in both identifications (A) and (B). The solid lines in Fig. 5-3 denote the fitting curves for each plot. It is very striking that the both curves are well reproducing the same numerical data. That is to say we cannot decide which is the correct scaling form Eq. (5·2) or (5·3), though Fig. 5-3 clearly reveals the existence of the scaling regime for each plot.

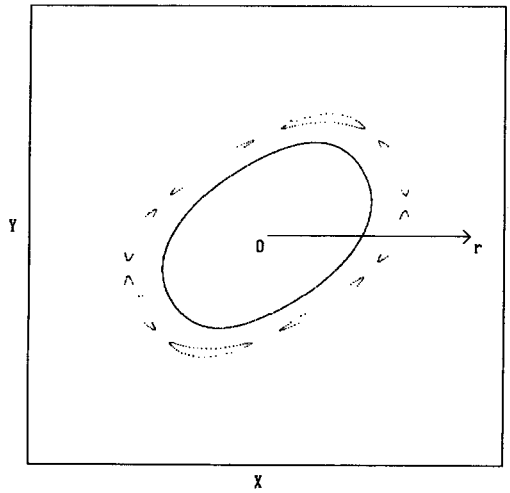

Fig. 5-4. The sketch of the standard mapping. The stagnant layer coordinate is measured along the r-axis in the figure.

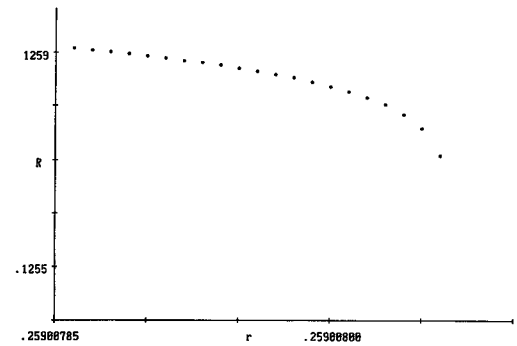

Fig. 5-5. The singularity of $R(r)$ in the standard mapping ($K/\pi=0.3$).

Standard map[27]

$$x'=x+y',$$
$$y'=y-(K/2\pi)\sin(2\pi x). \quad \text{(mod. 1)} \tag{5·4}$$
$$(K/\pi=0.3)$$

As is shown in Fig. 5-4, the distance r is measured from the elliptic center $(x, y)=(0, 0)$ along the x-axis. The final KAM surface is observed at $r=r_c$ $(=0.259008\cdots)$, above which the narrow chaotic band is generated due to the heteroclinicity of unstable cycles with the period 8. The critical point (r_c, R_c) is quite different from the previous example, but the qualitative aspect seems to be the same as seen in Fig. 5-2.

The best fitting by each scaling form of Eq. (5·2) or (5·3) was pursued in Fig. 5-5.

(A) $\alpha=0.141\cdots$, $\quad r_c=0.25900806437536\cdots$,

$R_c=0.1254320063\cdots$

and

(B) $\beta=0.775\cdots$, $\quad r_c=0.25900806460558\cdots$,

$R_c=0.125099421\cdots$.

Then existence of each scaling regime is shown in Fig. 5-6. In this example also we have not yet been able to decide the correct scaling form.

Tennyson map[24]

$$x'=x+0.1\tan(\pi y'),$$
$$y'=y-0.1\sin(2\pi x). \quad \text{(mod. 1)} \tag{5·5}$$

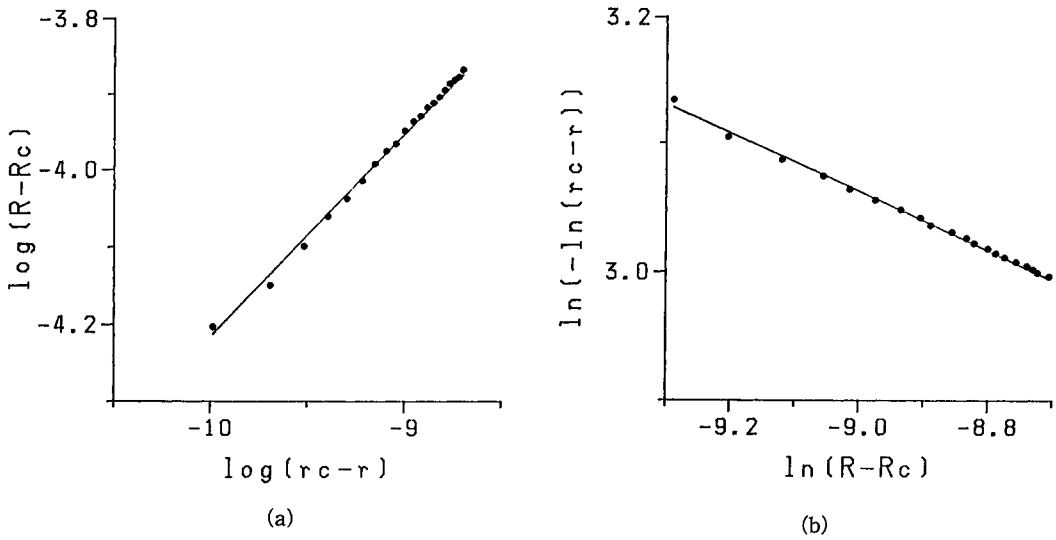

Fig. 5-6. The scaling regime for the standard map.
(a) Fitting by Eq. (5·2). (b) Fitting by Eq. (5·3).

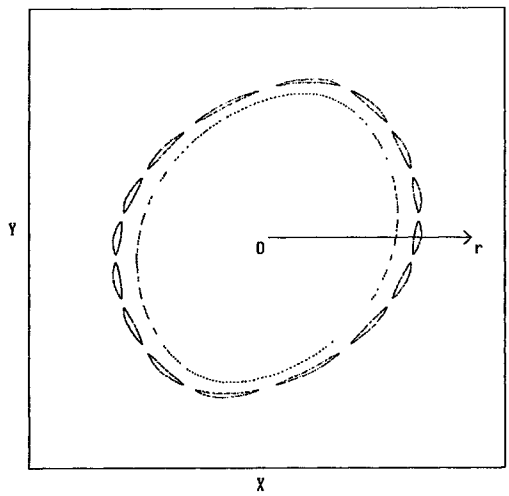

Fig. 5-7. The sketch of the Tennyson mapping. The stagnant layer coordinate is measured along the r-axis in the figure.

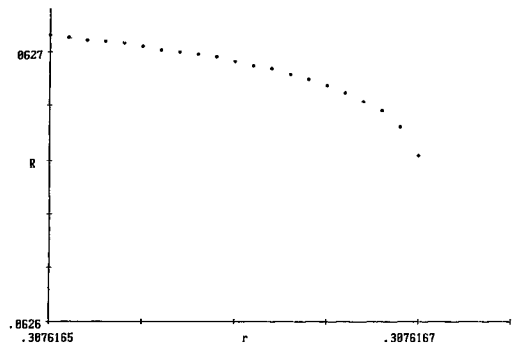

Fig. 5-8. The singularity of $R(r)$ in the Tennyson mapping.

The distance r is measured from the elliptic center $(x, y)=(0, 0)$ along the x-axis as illustrated in Fig. 5-7. The final KAM surface is observed at $r=r_c$ $(=0.30761\cdots)$, and the narrow chaotic zone is created by the heteroclinicity of unstable cycles with the period 16.

The rotation number is shown in Fig. 5-8, where the best fitting for each scaling form is obtained with the following parameters:

(A) $a=0.128\cdots$, $r_c=0.30761670614366\cdots$,

$R_c=0.062582655\cdots$

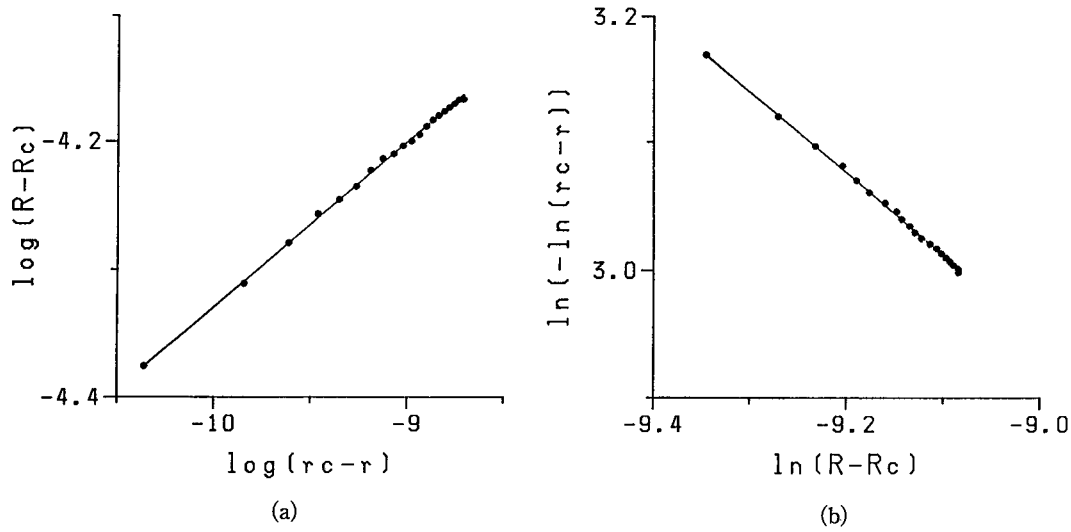

Fig. 5-9. The scaling regime for the Tennyson map.
(a) Fitting by Eq. (5·2). (b) Fitting by Eq. (5·3).

and

$$\text{(B)} \quad \beta=0.646\cdots, \qquad r_c=0.30761670614645\cdots,$$
$$R_c=0.062537420\cdots.$$

The scaling regime for each identification is shown in Fig. 5-9, where both plots seem to reproduce the numerical points as well.

Three examples treated in this section suggest the existence of a certain singularity at the final KAM surface, though we could not determine the scaling form definitely. We will close this section after giving two conjectures;

(i) Universality

The values of the critical indices for each example are rather close with each other. Therefore, if the scaling law is universal for that identification, the indices are roughly estimated as,

$$\alpha=0.13\pm0.015$$

or

$$\beta=0.77\pm0.11.$$

(ii) Singularity

Denoting the critical rotation numbers identified by Eqs. (5·2) and (5·3) by R_{CA} and R_{CB} respectively, and the rotation number in the adjacent chaotic band by R_χ, then the following ordering holds for every example,

$$R_{CA}>R_{CB}>R_\chi.$$

If the rotation number is a continuous function of r, i.e., the transition is not the first order type, the scaling form of Eq. (5·3) seems to be more plausible rather than Eq. (5·2). More precise calculations are still in progress.

§ 6. Model approach to the stagnant motions

In this section the basic formalism discussed in § 2 will be proved by carrying out with some simple models.

6.1. *Fractal geometrical model ——Two dimensional case——*

Let us consider the hierarchical distribution of the final KAM tori in phase space, where the final KAM of the i-th class is surrounded by the KAM islands of the $(i+1)$-th class as is illustrated in Fig. 2-3. The hierarchy is assumed to continue successively to the infinitesimal KAM islands in a self-similar manner. Precisely speaking, the phase space in each ghost separatrix C_i contains all the j-class KAM tori $K_j (j \geq i+1)$. Then the self-similar structure of the lexicographical tree is formed,

$$C_i = (K_i + K_{i+1} + \cdots) + (S_i + S_{i+1} + \cdots), \tag{6·1}$$

where S_j denotes the j-class chaotic zone,

$$S_j = C_j - C_{j+1} - K_j. \tag{6·2}$$

S_j is called the j-th class cluster for short, and all the chaotic motions occur in the union of the S_j's $(j=1, 2, \cdots)$. The self-similarity is assumed in the strict sense:

(1) One KAM torus of K_i is surrounded by ρ KAM islands of K_{i+1}, where ρ (>2) is a constant.

(2) The structure of the $(i+1)$-class cluster is similar with that of the i-class cluster, i.e., the volume ratio for each region is a constant b $(>\rho)$,

$$\frac{\mathrm{vol}(K_i)}{\mathrm{vol}(K_{i+1})} = \frac{\mathrm{vol}(S_i)}{\mathrm{vol}(S_{i+1})} = \frac{\mathrm{vol}(C_i)}{\mathrm{vol}(C_{i+1})} = b. \tag{6·3}$$

(3) The parameters ρ and b are constants independent of i, and the chaotic orbit in S_{i+1} is similar to that in S_i when the time course is measured at every ρ step.

When we assign the rank number l $(=0, 1, 2, \cdots)$ to every KAM torus in order of its volume, the phase volume of the l-rank torus v_l is described by,

$$v_l \sim l^{-1/D'}. \qquad (D' = \ln\rho / \ln b < 1) \tag{6·4}$$

Namely, the rank-size relation obeys the Pareto-Zipf law. From the above conditions, the followings are easily obtained.[60]

(i) The distribution of the volume $(v < v_l < v + dv)$ becomes,

$$P(v) \sim v^{-1+D'}. \tag{6·5}$$

(ii) The distribution of the pausing time n, during which the orbit stays in the i-th chaotic zone S_i and/or C_i becomes,

$$P(n) \sim n^{-D}. \qquad (D = 1/D') \tag{6·6}$$

This is independent of i. Besides the distribution of the first passage time $P(T)$, where T is the time necessary for an orbit to escape from a cluster C_i, is also

derived from the same consideration,

$$P(T) \sim T^{-D}. \tag{6·7}$$

Here the initial ensemble is assumed to be uniform in whole chaotic space $\mathrm{U}_{i=0}^{\infty} S_i$.

(iii) The power spectrum of the rotation angle around the 0-class torus K_0 becomes

$$S(f) \sim f^{-(3-D)}, \qquad (f \ll 1) \tag{6·8}$$

and its Allan variance $\sigma_A{}^2(n)$ becomes

$$\sigma_A{}^2(n) \sim n^{2-D}. \qquad (n \gg 1)$$

(iv) The fat fractal index μ, which was introduced by Umberger and Farmer,[59] becomes

$$\mu = 2(1-D'). \tag{6·9}$$

(v) The distribution of the Lyapunov exponent λ becomes

$$P(\lambda) \sim \lambda^{-(2-D)}, \tag{6·10}$$

where we used the temporal similarity, i.e., $\lambda_j \sim \rho^{-j}$.

Equations (6·5) and (6·10) can be used to predict the outlines of the stagnant motions. For instance, the pausing time distribution of Eq. (6·6) is compared with the Nekhoroshev estimation by putting $D=1$, and then $P(\lambda) \sim \lambda^{-1}$ and $S(f) \sim f^{-2}$ are predicted. These are consistent with the basic assumption used in the Nekhoroshev theorem, i.e., the nearly integrable limit ($D \fallingdotseq 1$).

The diffusion process in this model is described by the symbolic dynamics in the cluster space $\{S_i\}$, where the time course is traced by the number of the cluster $\{j\}$. For example, when the transition from S_j to S_k is limited to the nearest one, i.e., $k = j \pm 1$ and $k=j$, the symbolic dynamics is a simple random walk in the cluster space. Assuming the detailed balance for the jump process, the transition probability $P_{j,k}$ (from j to k) is obtained[60]

$$P_{j,k} \sim (\rho/b)^{k-j}. \tag{6·11}$$

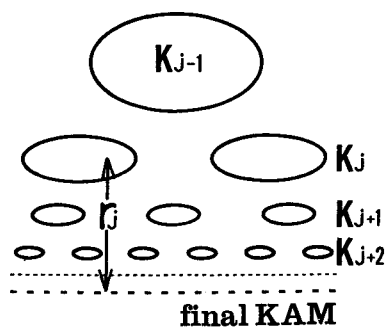

Fig. 6-1. The multiple layer model near the final KAM surface. r_j denotes the distance to the j-th layer.

This implies that an orbit is liable to flow from the micro-cluster to the outside, e.g., $P_{j,j+1} > P_{j+1,j}$.

The model discussed so far is so-called "islands around island". But the basic idea is also applicable to another geometrical structure, i.e., as is illustrated in Fig. 6-1 we assume the hierarchical series of KAM islands is accumulating towards the final KAM surface when the cluster number j increases to infinity.[85),104),105] If the distance r_j from the final KAM surface to the j-

cluster islands is an exponential function of j,

$$r_j = r_c + (1/b')^j, \qquad (b'>1) \tag{6·12}$$

then the equilibrium distribution of the symbolic j-state $P_j(=(\rho/b)^j)$, which is proportional to the phase volume, is transferred to the invariant measure in the r-space $P(r)$,

$$\begin{aligned} P(r) &\sim (r-r_c)^{-1}(\rho/b)^{-\ln(r-r_c)/\ln b'} \\ &\sim (r-r_c)^{-\alpha} \end{aligned} \tag{6·13}$$

with $\alpha = \ln(b/\rho)/\ln b' + 1$. Here $r = r_c$ stands for the final KAM surface. Therefore, the integrability limit ($D=1$) corresponds to $\alpha = 1$.

The above discussion can be applied to the critical phenomena of the last KAM surface;[85] the KAM islands with the Fibonaccian cycle obey the same scaling as Eq. (6·13) by putting,

$$\rho = \text{golden mean} \tag{6·14}$$

and

$$\rho^j = j\text{-th Fibonacci number for large } j,$$

and then b' is a universal constant as was predicted by Greene.[49),53),57)]

6.2. *One dimensional model*

The modified Bernoulli map is the most simple system which generates the stagnant motion,[111),112)]

$$X' = \begin{cases} X + 2^{B-1}X^B, & (0 \le X \le 1/2) \\ X - 2^{B-1}(1-X)^B, & (1/2 \le X \le 1) \end{cases} \tag{6·15}$$

where B stands for the intensity of the stagnant effect. In the case $B > 3/2$, the orbit stays for long time in the stagnant region near the fixed points $X=0$ and $X=1$. As was proved in the previous papers, the distribution of the pausing time n in each stagnant region $P(n)$ obeys,[111),112)]

$$P(n) \sim n^{-\beta}, \tag{6·16}$$

and the power spectrum $S(f)$ becomes,

$$S(f) \sim f^{-(3-\beta)} \tag{6·17}$$

with $\beta = B/(B-1)$. The invariant measure $P(X)$ becomes singular,

$$P(X) \sim \begin{cases} X^{-(B-1)}, & (X \cong 0) \\ (1-X)^{-(B-1)}. & (X \cong 1) \end{cases} \tag{6·18}$$

As the result, the local Lyapunov exponent λ is zero for $B \ge 2$, and the distribution of λ is given by

$$P(\lambda) \sim \lambda^{-(3-\beta)}. \qquad (\lambda \ll 1) \tag{6·19}$$

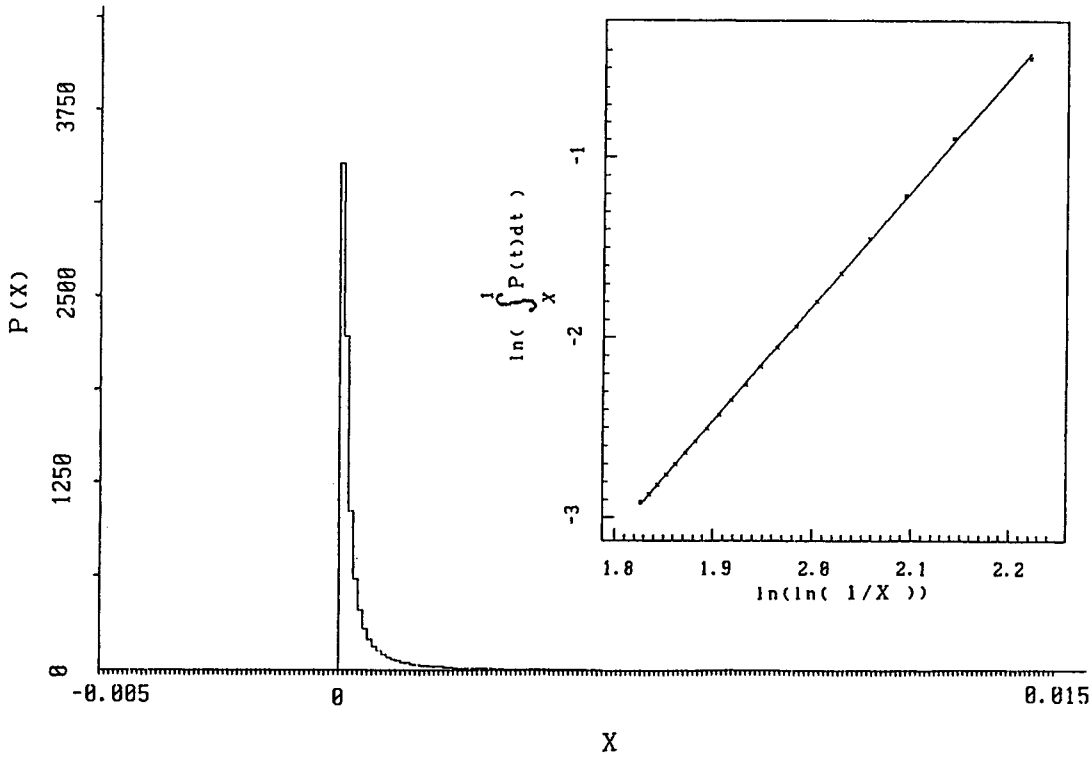

Fig. 6-2. The invariant measure for the one dimensional mapping of Eq. (6·20) with $A=0.6$ and $\varepsilon=10^{-5}$.

The modified Bernoulli map is too simple to reproduce the complex behaviors of hamiltonian systems. A weak point is that this model does not take account of the fractal structure of "islands around island" as was discussed before. Here we go back to the numerical result illustrated in Fig. 3-6. By using the stagnant layer coordinate r, the successive return map $(r \to r')$ is approximated as,

$$r'=r+Ar\sin(\pi/r)+\varepsilon(1-r)\,, \qquad (0\leq r\leq 1) \tag{6·20}$$

following the previous discussion. Here A is a parameter and $\varepsilon(\ll 1)$ small perturbation. The second term of the r.h.s. represents the hierarchy of the KAM islands which are accumulating towards the final KAM surface at $r=0$. Figure 6-2 shows the numerical result of the invariant measure $P(r)$, which is precisely adjustable by

$$P(r)\sim(1/r)\Big[\ln(1/r)\Big]^{a}\,. \qquad (a\fallingdotseq 5.3) \tag{6·21}$$

This seems to be consistent with Eq. (6·13) with $a=1$.

6.3. *Stochastic model*

In order to understand the diffusion process in a stagnant layer, the following stochastic analog is useful:

$$dr/dt=R(t)(r-r_1)(r_2-r)\,, \tag{6·22}$$

where $R(t)$ is a white gaussian noise and the motion is assumed to be trapped in the

region $r_1 < r < r_2$. The orbit can escape from the stagnant layer when r_2 goes to infinity. If the variable r denotes the energy of a normal mode E_1 as was discussed in § 4, the model of Eq. (6·22) may represent the Arnold diffusion process. But in what follows, we consider a chaotic band that is sandwiched by two final KAM surfaces located at $r=r_1$ and $r=r_2$.

Defining a new variable Y by

$$Y=\ln\{(r-r_1)(r_2-r)/(r_0-r_1)(r_2-r_0)\}\,, \tag{6·23}$$

$Y(t)$ is the Wiener process and the transition probability $P(Y, Y_0; t)$ satisfies,

$$P(Y, Y_0; t)\sim\exp[-(Y-Y_0)^2/2t]\,, \tag{6·24}$$

where r_0 stands for the initial value of r and $Y_0=0$. As the result, the equilibrium distribution $P(r)$ satisfies,

$$\begin{aligned} P(r)&\sim 1/(r-r_1)+1/(r_2-r) \\ &\sim 1/(r-r_1)\,. \quad (r_2\to\infty) \end{aligned} \tag{6·25}$$

This is the same scaling form used in § 2.

As shown in the above argument, the stochastic analog discussed here well reproduces the scaling relations used in § 2.3, but the essential difference must be noticed and the Arnold diffusion must be compared with more complex models. When we use the following analog:

$$dr/dt=R(t)(r-r_1)\,, \tag{6·26}$$

the variable $X(t)$ $(=\ln\{(r-r_1)/(r_0-r_1)\})$ becomes the Wiener process. Comparing with Eq. (6·12), $X(t)$ corresponds to the coordinate $j(t)$ of the symbolic state $\{j\}$, i.e.,

$$\{j(t)-j(0)\}\ln b'\sim -X(t)\,. \tag{6·27}$$

Therefore, the first passage time T necessary for an orbit to cross a certain level of $r=r_T$ (=constant) obeys the following distribution $P(T)$:

$$\begin{aligned} P(T;r=r_T)&\sim\int_0^\infty z/T^{3/2}\exp(-z^2/2T)dz \\ &\sim T^{-1/2}\,, \qquad (T\gg 1) \end{aligned} \tag{6·28}$$

where we used the first passage time distribution for the Wiener process[90] and the uniform initial ensemble, i.e., $P(j)\sim(\rho/b)^j\sim$const or $P(r)\sim(r-r_1)^{-1}$ as was obtained in Eq. (6·13). Equation (6·28) is not consistent with the result obtained in § 2. In the present analog we assumed that the time scale of the white noise $R(t)$ is taken to be uniform and not to depend on $r(t)$. But this assumption is not correct and we have to consider the effect of the critical slowing down in the neighborhood of the final KAM torus at $r=r_1$. The mechanism of such critical slowing down has not yet been clear, but it might be correlated to the breakdown of the markoffian assumption used in Eq. (6·13).[89] These are still open.

§ 7. Multi-ergodic features of the large scale diffusion

In the previous sections we have mainly discussed the local aspects of the stagnant motion around a single KAM torus, but in this section the global features in whole chaotic space will be studied. In general, infinite number of KAM islands are very complicatedly distributed in phase space, and that every final KAM torus is wrapped up with the inherent stagnant layer. Therefore, one chaotic orbit is slowly passing by the arbitrary vicinity of every final KAM torus. The purpose of this section is to discuss the ergodic problems of such wandering motions in the large.

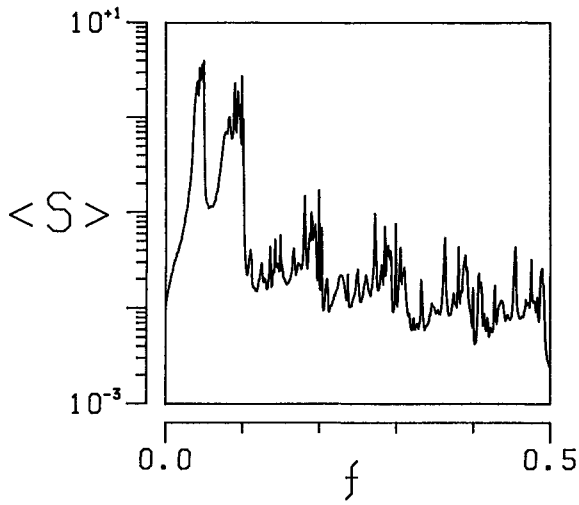

Fig. 7-1. The mean power spectrum $\langle S(f)\rangle$ of the variable x for the standard map (Eq. (5·4)) with $K=0.5$ and $N=10^4$.

7.1. *Multi-ergodicity and non-stationarity*

The pausing time distribution in the i-th stagnant layer $P_i(T)$ ($i=1, 2, \cdots$) satisfies,

$$P_i(T) \sim T^{-\beta_i} \tag{7·1}$$

and the power spectral density (PSD) function $S(f)$ becomes,

$$S_i(f) \sim |f-f_i|^{-\nu_i} \tag{7·2}$$

with $\nu_i=3-\beta_i$, where f_i stands for the characteristic frequency of the i-th

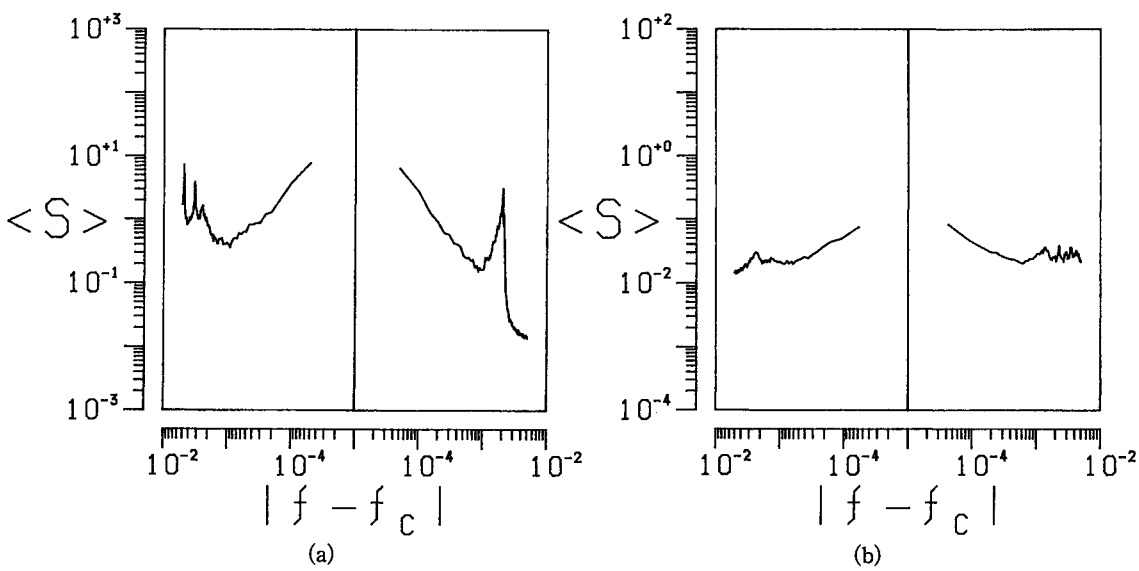

Fig. 7-2. The spectral singularity at the resonant frequency f_c. $\nu_\pm$ stands for the spectral index for $f \gtrless f_c$. (a) For $f_c=1/10$ ($\nu_+=1.04$, $\nu_-=1.21$). (b) For $f_c=1/7$ ($\nu_+=0.60$, $\nu_-=0.58$).

final KAM torus. Therefore the PSD function of the chaotic orbit in the large $\langle S(f)\rangle$ must be,

$$\langle S(f)\rangle=\sum_i A_i|f-f_i|^{-\nu_i}+(\text{regular part}), \tag{7·3}$$

where the A_i's denote the relative intensity and $\langle\ \rangle$ implies the ensemble average due to the asymptotic measure for one orbit under consideration. The results in the previous sections persist that the indices are uniquely determined as $\beta_i=1$ and $\nu_i=2$ for the pure stagnant motion. But in what follows, the values of these indices are considered to be parameters, since it is difficult to get the perpetually stagnant orbit in the numerical simulation even if the calculation time is infinitely long. The singular spectrum is often observed in the numerical simulation, but here in this section Eq. (7·3) must be considered to be a hypothesis.

Figure 7-1 is the PSD function of one chaotic orbit in the standard mapping, where we can see a lot of singularities as is described by Eq. (7·3). However, the spectral indices ν_i's are usually less than 2, and that the scaling form is not always symmetric around the characteristic frequency f_i (see Fig. 7-2). The difference between the numerical results and the theoretical prediction seems to come from the restriction in machine calculations such that the time series used is very long but finite. Namely, the orbit cannot get into the deep inside of each stagnant layer, but only skims over each layer during a finite period. To detect the critical effect arising from every stagnant layer we have to treat the time series of infinite length rigorously. Here we are confronted with two essential difficulties which cannot be solved in the simple ergodic-theoretical framework. The first one is the break-up of the recurrence property, i.e., the mean residence time in each stagnant layer becomes infinity,

$$\langle T_i\rangle=\int TP_i(T)dT\longrightarrow\infty \tag{7·4}$$

for $\beta_i\leq 2$ in Eq. (7·1). The second comes from the fractal distribution of KAM islands, i.e., the number of singular frequencies f_i's in Eq. (7·3) is never countable infinity but uncountable just like a cantor set. From these considerations it is possible to derive the following two general aspects for the global chaos in hamiltonian systems:

(i) Multi-ergodicity

The recurrence property (in the sense of Poincaré) breaks down in every stagnant layer, and the asymptotic measure defined in each layer is mutually independent from the others if all the stagnant layers are topologically connected by some orbits. One of the most natural measures in the area-preserving system is the Lebesgue measure. However, in each stagnant layer the most dominant one of them is not the Lebesgue measure, but is the inherent asymptotic measure that is strongly localized near the final KAM torus as was discussed in § 2. We call the coexistence of such local measures "multi-ergodicity" for short.

(ii) Non-stationarity

As the result of the multi-ergodicity, the time average of a dynamical variable (e.g., denote the average of the variable X by $\bar{X}$) is strongly dependent of the initial

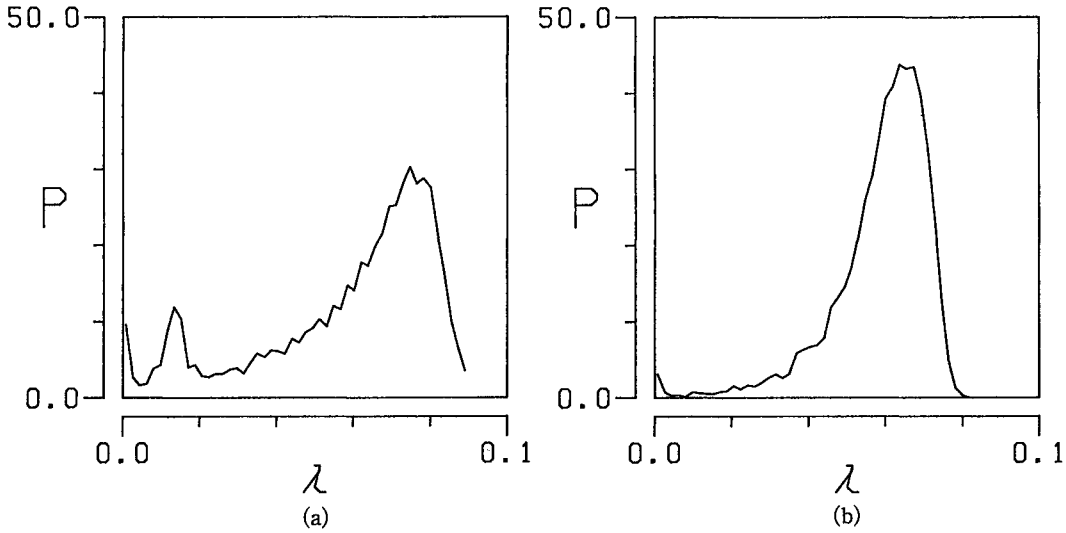

Fig. 7-3. The distribution of the Lyapunov exponent $P(\lambda)$.
(a) For $T=10^5$. (b) For $T=10^6$.

data or the asymptotic measure. The time course $X(t)$ is stationary if the probability distribution of the partial average $\bar{X}_T$ defined by

$$\bar{X}_T=1/T\int_0^T X(t)dt\,, \tag{7·5}$$

converges exponentially to a constant $\bar{X}$ as T goes to infinity, i.e.,

$$P(\bar{X}_T)\longrightarrow\delta(\bar{X}_T-\bar{X})\,,\qquad (T\to\infty) \tag{7·6}$$

where $\delta(\cdot)$ denotes the delta function. However, in the multi-ergodic system we cannot expect such uniform convergence in unique, since the mean pausing time in each stagnant layer becomes infinity. In other words, the weak law of large number is violated in the multi-ergodic system and the stationarity is lost.[98),99)]

The essence of the multi-ergodicity and the non-stationarity in hamiltonian systems must be reasonably understood in the framework of *the large deviation theory*.[68)] The coexistence of the local asymptotic measures corresponds to the non-uniqueness of the Gibbs state or the coexistence of the thermodynamical phases. The similarity between the multi-ergodic dynamical system and the critical phenomena in statistical mechanics will be discussed later.

The extremely slow convergence of the time average $\bar{X}_T$ in Eq. (7·5) is often observed in the multi-ergodic system. As an example, the distribution of the Lyapunov exponent $\bar{\lambda}_T$ defined by

$$\bar{\lambda}_T=1/T\ln\left|\frac{\boldsymbol{e}(T)}{\boldsymbol{e}(0)}\right| \tag{7·7}$$

is shown in Fig. 7-3, where $\boldsymbol{e}(s)$ stands for the tangent vector at the time $t=s$. At $T=10^5$ the distribution reveals three dominant peaks that correspond to macroscopic

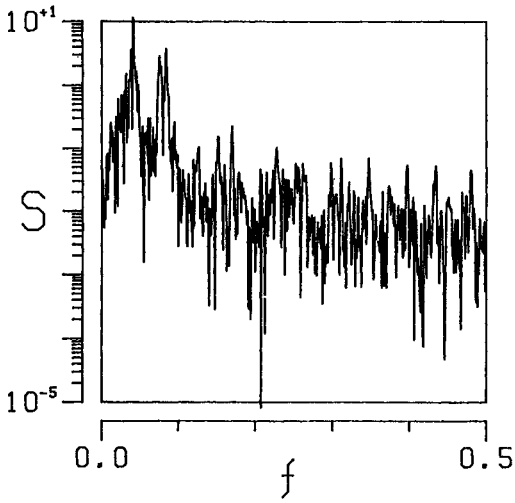

Fig. 7-4. A path dependent power spectrum $S(f)$ corresponding to Fig. 7-1.

phases.[115] If they survive even in the limit $T\to\infty$, the phase coexistence can be expected. However, two of them gradually decreases as T goes to large. The remarkable point is that the lowest peak around $\lambda=0$ obeys the inverse power law,

$$P(\lambda)\sim\lambda^{-a}\ (\text{with } a\fallingdotseq 0.35)\,, \qquad (7\cdot 8)$$

in line with the argument in § 2. Besides the middle peak disappears very slowly and the dominant peak becomes unique. The convergence of the Lyapunov exponent is very curious, and the simple ergodic theorem by Oseledec must be revisited from the viewpoint of the multi-ergodicity.[7]

7.2. *Multi-fractal approach to the PSD function*

We consider two kinds of PSD functions; one is the path-dependent PSD ($S(f)$) which is usually unstable and robust as is shown in Fig. 7-4, and another is the mean PSD ($\langle S(f)\rangle$) that is obtained from the ensemble average on the asymptotic measure of one orbit. If the system is simply ergodic, the asymptotic measure converges to a stationary one, and then $\langle S(f)\rangle$ approaches to a rather smooth function as is predicted in the large deviation theory.[117] But in the non-stationary multi-ergodic case which we are discussing here, $\langle S(f)\rangle$ is still fluctuating and robust as is shown in Fig. 7-1.

Denoting the length of each sample path by N, the resolution of the frequency is $1/N$. When we box the frequency domain into boxes of size Δ, the intensity in the i-th box Δ_i is scaled as,

$$S_i(\Delta)=\int_{f\in\Delta_i}\langle S(f)\rangle df\sim\Delta^{\mu_i}\,, \qquad (7\cdot 10)$$

provided that $\langle S(f)\rangle$ has a singularity in the box,

$$\langle S(f)\rangle\sim|f-f_i|^{-\nu_i}\,,\quad (\nu_i<1,\, f_i\in\Delta_i) \qquad (7\cdot 11)$$

with $\mu_i=1-\nu_i$. When ν_i is less than zero, the frequency f_i stands for the absorption line. Here we assume that $\langle S(f)\rangle$ is the probability density in frequency domain, i.e., $\int\langle S(f)\rangle df=1$. Then the multi-fractal analysis is used to determine the fluctuation of the local dimension μ.[114] The distribution of the singularity index, $P(\mu)\sim\Delta^{-\tilde{F}(\mu)}$, is derived by the Legendre transformation of the q-order dimension D_q,

$$\tilde{F}(\mu)=q\mu-(q-1)D_q \qquad (7\cdot 12)$$

and

$$D_q=\frac{1}{q-1}\frac{\ln\sum S_i(\Delta)^q}{\ln\Delta}\,, \qquad (7\cdot 13)$$

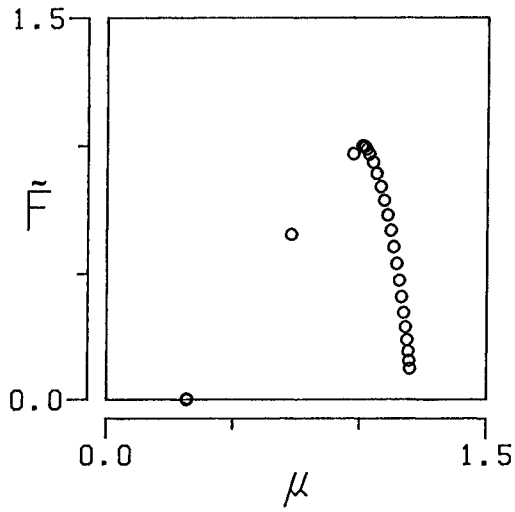

Fig. 7-5. The multi-fractal spectrum $\tilde{F}(\mu)$ corresponding to Fig. 7-1.

where $\mu=d/dq[(q-1)D_q]$.

The following relations are used in the numerical analysis by putting $\Delta \sim 1/N$,

$$D_q=I_q/\ln N$$

and

$$I_q=\frac{1}{1-q}\ln\sum_i S_i^q\,,$$

under the scaling assumptions,

$$S_i=N^{-1}\langle S(f)\rangle_{f=i/N}\sim N^{-\mu_i}\,.$$

I_q is the generalized Renyi's spectral entropy.[118] Figure 7-5 is the dimension spectrum $\tilde{F}(\mu)$.

The spectral index μ is corresponding to the local dimension if $\nu<1$ holds, but for the non-stationary case $\nu>1$ the relation $\mu=1-\nu$ must be discarded. So in what follows, we must consider the value of μ is only a scaling index defined by Eq. (7·10).

The most dominant dimension μ^* is obtained from the relation $\tilde{F}(\mu^*)=\mu^*$, i.e., $\mu^*=0.98$, and the minimum and the maximum values are numerically determined, $\mu_{\min}=0.32$ and $\mu_{\max}=1.20$ respectively. The multi-fractal analysis of $\langle S(f)\rangle$ is useful for the better understanding of the multi-ergodic motion. To compare with simple ergodic motions, let us consider the K-system defined by[63]

$$\begin{aligned} X'&=X+Y\,,\\ Y'&=X+2Y\,. \qquad \text{(mod. 1)} \end{aligned} \tag{7·14}$$

The power spectral density of X-variable $\langle S(f)\rangle$ becomes white, and the multi-fractal spectrum $\tilde{F}(\mu)$ is sharply localized at $\mu=1$, that corresponds to the fact that the dominant ergodic measure is unique in this system. The multi-fractal analysis were successfully used for the characterization of the multi-ergodic motion, but the essential difference between both ideas, multi-fractals and multi-ergodicity, must be recognized. The multi-fractal spectrum characterizes a single measure on a certain fractal set in phase space. On the other hand, in the multi-ergodic system the global asymptotic measure is not a single but compound of the non-stationary ones as was discussed before. As the result, the dimension spectrum $\tilde{F}(\mu)$ depends on the orbit ρ under consideration; $\tilde{F}(\mu)=F_\rho(\mu)$. Roughly speaking, the result shown in Fig. 7-5 is the mean spectrum $\langle F_\rho(\mu)\rangle$, where $\langle\ \rangle$ denotes the ensemble average on the path space $\{\rho\}$. The dimension spectrum $F(\mu)$ was introduced by Procaccia as a measure which characterizes the fluctuation of local dimension μ in a simple ergodic component. But in the multi-ergodic system we have to discuss the fluctuation of $F(\mu)$ itself.

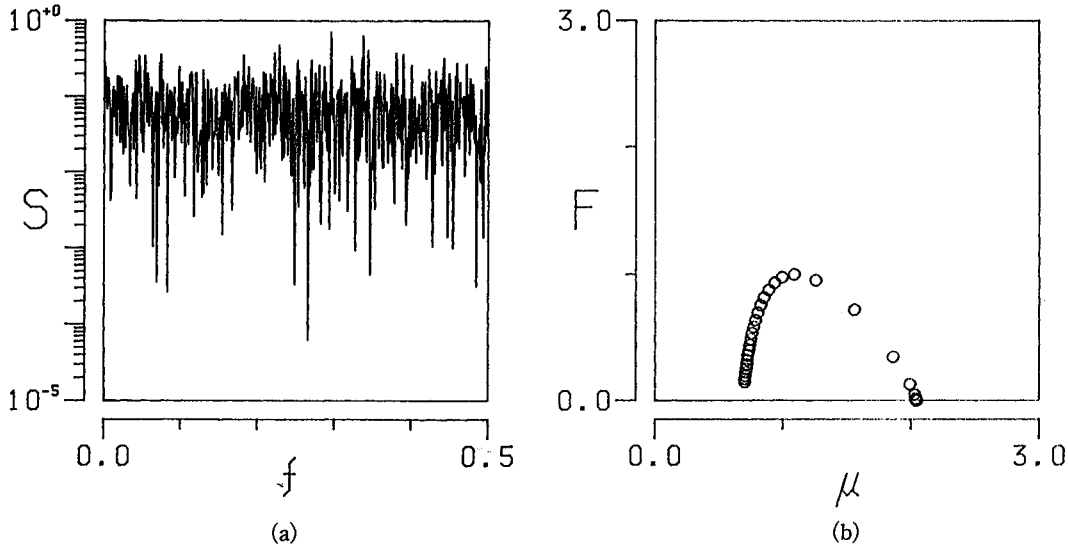

Fig. 7-6. The path dependent $S(f)$ and $F_\rho(\mu)$.
(a) The path dependent power spectrum $S(f)$ for the strong ergodic system of Eq. (7·14).
(b) The multi-fractal spectrum $F_\rho(\mu)$ corresponding to (a). The spectrum $F_\rho(\mu)$ is insensitive to the path.

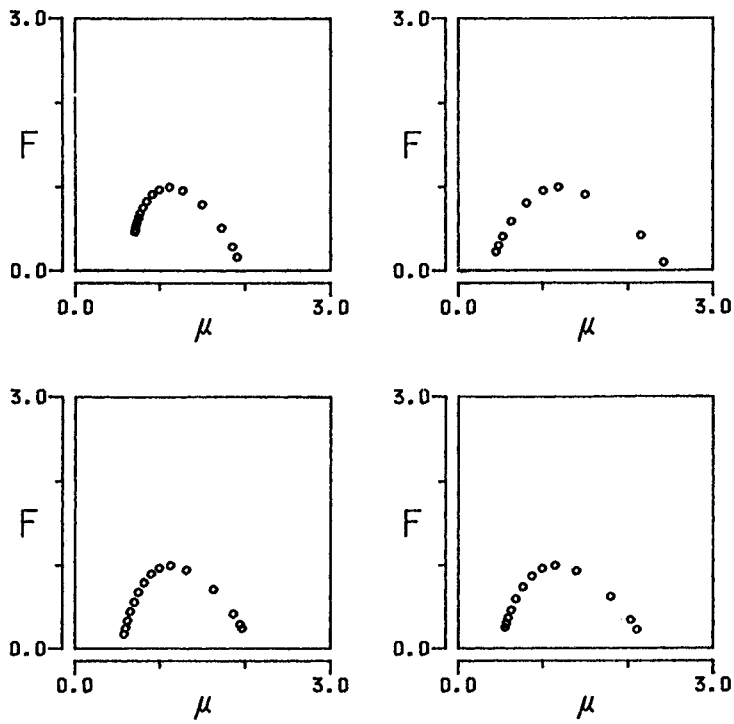

Fig. 7-7. The multi-fractal spectrum $F_\rho(\mu)$ of the standard map corresponding to Fig. 7-4. The four samples ($\rho=1\sim4$) are illustrated for $N=10^4$.

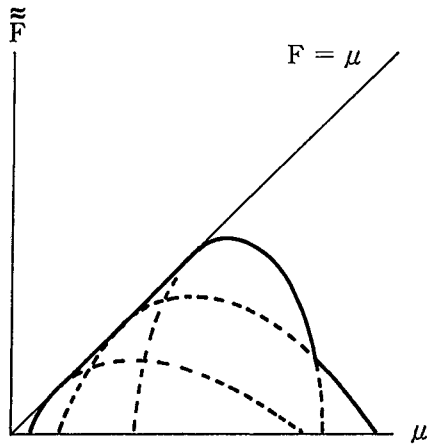

Fig. 7-8. The schematic picture of the multi-fractal spectrum $\tilde{\tilde{F}}(\mu)$ for the multi-ergodic system.

7.3. *Fluctuation of the dimension spectrum*

We come back to path dependent PSD function $S(f)$ in Fig. 7-4. In general, $S(f)$ is quite robust if the average $\langle S(f)\rangle$ is smooth. For instance, the PSD function of the K-system described by Eq. (7·14) is considered. The dimension spectrum $F_\rho(\mu)$ for the path dependent PSD is shown in Fig. 7-6, where we used the same method as before. The fine structure of $S(f)$ is sensitively dependent on the initial data for each path, but the over-all behavior of $F_\rho(\mu)$ is almost insensitive on the sample path. In other words, the fluctuation of the spectrum is negligibly small for the simple ergodic motion like K-system.

When the same analysis is applied to the previous example of Fig. 7-4, the remarkable effect of fluctuations is observed as is shown in Fig. 7-7, where the dimension spectra are illustrated for 4 sample paths. The dominant dimension μ^* $(=F_\rho(\mu^*))$ is fluctuating $(0.75<\mu^*<0.93)$, besides the forms of $F_\rho(\mu)$'s are quite different. Though the path length $N(=10^4)$ is not so large in the present simulations, the non-stationary aspect of the multi-ergodicity seems to be elucidated at least qualitatively. If we consider all of the possible asymptotic measures, the maximal dimension spectrum $\tilde{\tilde{F}}(\mu)$ would be defined by the envelope of every path-dependent one as is illustrated in Fig. 7-8. $\tilde{\tilde{F}}(\mu)$ is the locally convex function and the dominant dimension μ^* $(=\tilde{\tilde{F}}(\mu^*))$ is continuously distributed for $\mu_1<\mu^*<\mu_2$. In terms of the large deviation theory, this situation means the non-uniqueness of the Gibbs state or the coexistence of many thermodynamical phases. The analogy with the critical phenomena in statistical mechanics will be further pursued in what follows.

7.4. *Anomalous large deviation*

The fluctuation of the spectral power is measured by the variance defined by

$$\langle \Delta S(f)^2\rangle=\langle S(f)^2\rangle-\langle S(f)\rangle^2 . \tag{7·15}$$

We often observe that the fluctuation is anomalously enhanced at the singular frequency f_i's, i.e., $\langle S(f)\rangle\sim|f-f_i|^{-\nu_i}$, though the fluctuation is rather normal at the non-singular frequency. Figure 7-9 shows the distribution of the spectral power at $f=1/7$ in the simple ergodic system defined by Eq. (7·14), where every frequency component is not singular. The result is well adjustable by the Γ-distribution,

$$P(x)=(1/\Gamma(\eta))x^{\eta-1}\exp[-x] , \qquad (\text{with } \eta=1) \tag{7·16}$$

under an appropriate scale transformation of $x\propto S(f)$. Denoting the fourier component of the time series by the complex value $C(f)=A(f)+iB(f)$,

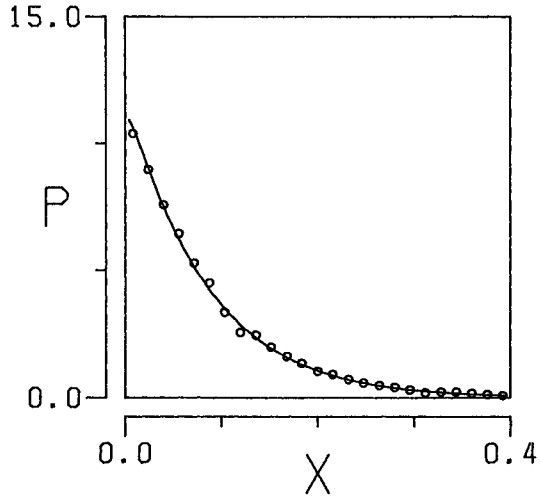

Fig. 7-9. The distribution of the spectral power at $f=1/7$ for the strong ergodic case corresponding to Fig. 7-6. The solid line is the fitting by Eq. (7·16).

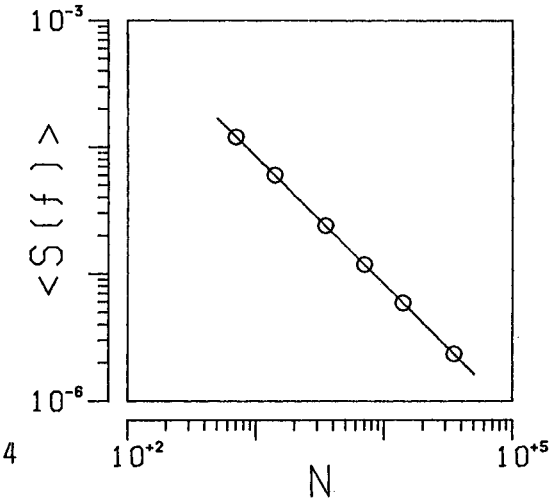

Fig. 7-10. The normal large deviation property for the strong ergodic case corresponding to Fig. 7-9.

$$S(f)=|A(f)|^2+|B(f)|^2 . \tag{7·17}$$

When the random variables A and B obey the mutually independent same gaussian distribution, the distribution of $S(f)$ obeys Eq. (7·16). Indeed, the distributions of A and B are well adjustable by the identical gaussian. When we define the partial sum $C(f)$ from the time series x_n,

$$C(f)=(1/N)\sum_{n=1}^{N} x_n \exp[-i2\pi jn/N] , \qquad (\text{with } f=j/N) \tag{7·18}$$

the large deviation of A (and B) is expected to yield the normal exponential convergence, i.e.,

$$P(A)\sim\exp[-N^{\delta}\mathcal{F}(A)] , \qquad (\text{with } \delta=1 , \text{ for large } N) \tag{7·19}$$

where $\mathcal{F}(A)$ is so-called "entropy". Namely, in the system of Eq. (7·14),

$$\mathcal{F}(A)\sim A^2 . \tag{7·20}$$

Therefore, the variance $\langle \Delta S(f)^2\rangle$ and the average $\langle S(f)\rangle$ satisfy,

$$\langle \Delta S(f)^2\rangle \sim O(N^{-2})$$

and

$$\langle S(f)\rangle \sim O(N^{-1}) , \tag{7·21}$$

respectively. The numerical result is consistent with this scaling as is shown in Fig. 7-10.

Next we apply the same analysis to the multi-ergodic case of Fig. 7-4. Then the distribution of $X=|C(f)|^2$ ($\propto S(f)$) is adjusted by

$$P(X)\sim X^{\eta-1}\exp[-\Psi(X)] \tag{7·22}$$

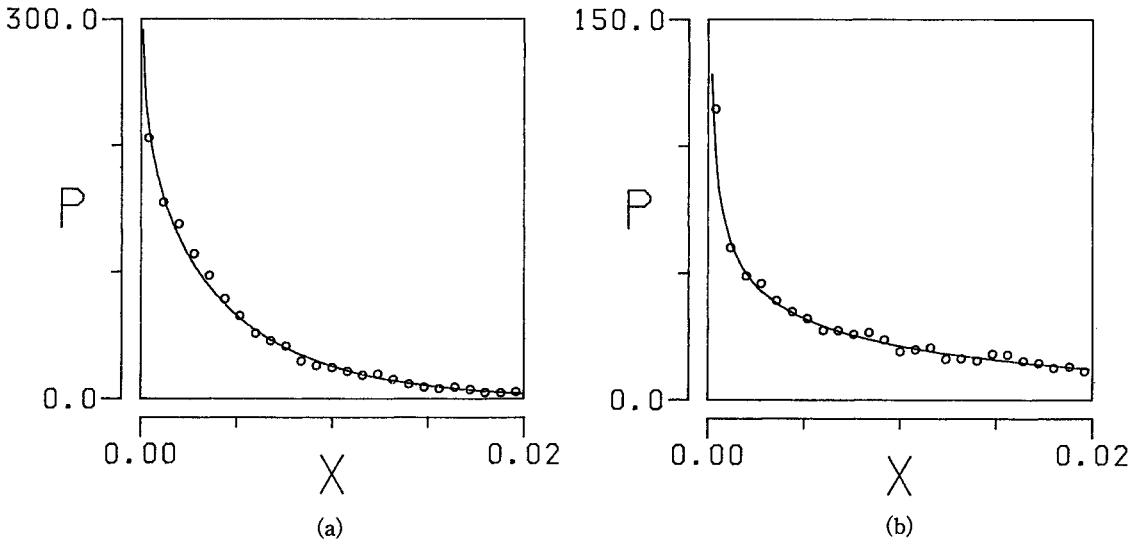

Fig. 7-11. The distribution of the spectral power for the standard map corresponding to Fig. 7-1. The solid line is the fitting by Eq. (7·22) with $X=|C(f)|^2$.
(a) For the non-singular component at $f=13/250$ ($\eta\fallingdotseq 0.85$, $\zeta\fallingdotseq 1.11$).
(b) For the singular component at $f=1/7$ ($\eta\fallingdotseq 0.62$, $\zeta\fallingdotseq 0.71$).

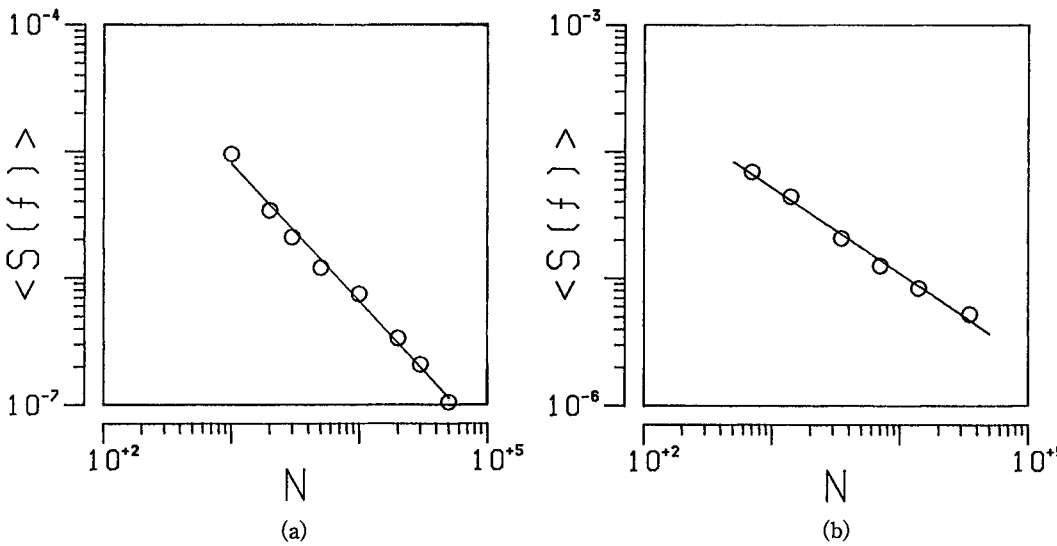

Fig. 7-12. The anomalous large deviation properties for the standard map corresponding to Fig. 7-11.
(a) $f=13/250$ ($\xi\fallingdotseq 1.11$), (b) $f=1/7$ ($\xi\fallingdotseq 0.68$).

with the entropy $\Psi(X)\sim N^{\zeta}X$. (Fig. 7-11(a), (b)). The corresponding mean value $\langle S(f)\rangle$ obeys the following scaling:

$$\langle S(f)\rangle\sim O(N^{-\xi}) \tag{7·23}$$

as is shown in Figs. 7-12(a) and (b). The non-singular frequency at $f=13/250$ reveals

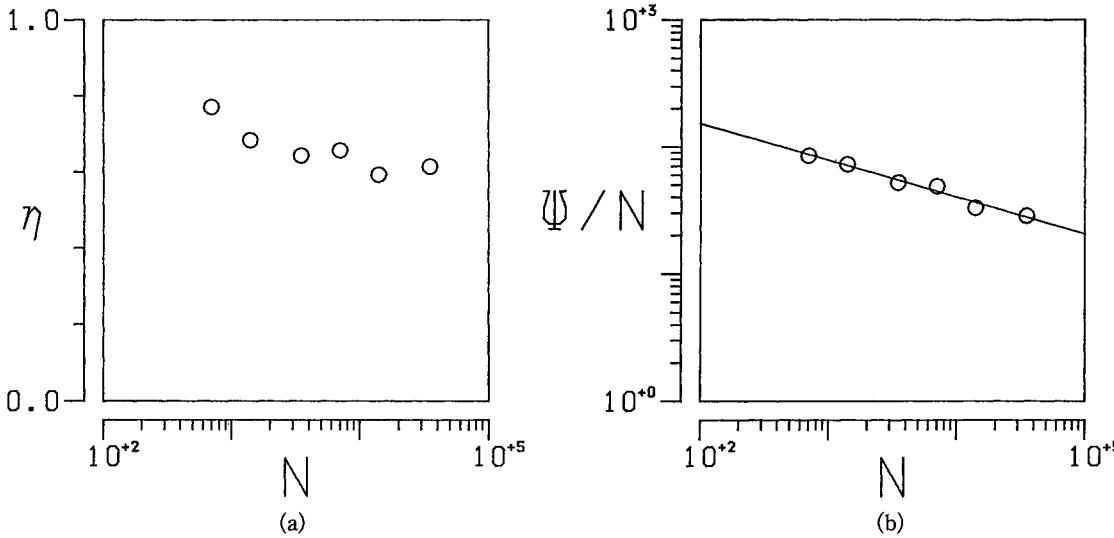

Fig. 7-13. The indices η and ζ at the singular frequency $f=1/7$ for the standard map corresponding to Fig. 7-11.
(a) N-dependence of η. (b) N-dependence of $\Psi(\zeta \fallingdotseq 0.71)$.

an accellerated convergence ($\zeta>1$), but a very slow convergence appears at the singular frequency, e.g., $\zeta<1$ for $f=1/7$. The origin of the former accellerated convergence is still unknown, but it might be understood as the counter effect due to the enhancement of the singular frequency components. The fact that the convergence of the spectral power is quite slow in comparison with the normal case of Eq. (7·19) implies that the random variables A and B are not mutually independent but are strongly correlated at the singular frequencies f_i's. These aspects seem to be consistent with the fact that each spectral singularity is created by the very slow diffusion in the corresponding stagnant layer in phase space. This is compared with the critical slowing down near the phase transition point.

The coherence between the real and imaginary parts of $C(f)$ in Eq. (7·18) is measured by the index η in Eq. (7·16); the value of 2η is called the degree of freedom in the chi-square test. The case $\eta=1$ implies the mutual independence of A and B, and $\eta=1/2$ for the complete coherence ($A=B$). In general, the real and imaginary parts are partially coherent $0.5<\eta<1$, and the phase variable φ defined by $\varphi=\tan^{-1}(B/A)$ is not random. Indeed, the value of η is rather insensitive to N, and the example of Figs. 7-13(a) and (b) reveals the partial phase locking, i.e.,

$$\eta \fallingdotseq 0.62\,, \qquad (\text{for } f=1/7)$$
$$\eta \fallingdotseq 0.85\,. \qquad (\text{for } f=13/250) \tag{7·24}$$

The appearance of such phase order is a characteristic phenomenon of the multi-ergodic motions. The mean value $\langle S(f)\rangle$ is calculated from Eq. (7·22),

$$\langle S(f)\rangle \sim O(N^{-\xi})\,. \tag{7·25}$$

This is compared with Eq. (7·23), i.e., $\xi \fallingdotseq \zeta$. The numerical error is less than few

percents.

It is surmised that the anomalous large deviation is induced by the phase coherence of Eq. (7·24) and the index ζ might be determined by η, but the correlation is still unknown. The multi-ergodic aspects of hamiltonian systems will be further discussed in the forthcoming paper.[120)]

§ 8. Summary and discussion

In this paper we have tried to elucidate the origin of the long time tails in hamiltonian dynamics, and tried to explain the stagnant phenomena in terms of the critical phenomena. The parallelism (between the stagnant motion and the critical fluctuation in statistical mechanics) is partially confirmed at least in the phenomenological framework, but the consistent theory has not been sufficiently developed here. These problems are left in future, but here the parallelism will be emphasized again. The Nekhoroshev bound T is the most essential quantity which characterizes a coherent length of the chaotic motion, and the control parameter is the distance r in the action space. Equation (2·23) is rewritten into

$$T \sim |r-r_c|^{-\gamma}, \tag{8·1}$$

where r_c stands for the critical point, and γ is a critical exponent. This is the same expression for the critical regime of the phase transition. In this paper, we have used Eq. (8·1) only for $r>r_c$, but the same relation is surmised to hold in the sub-critical region ($r<r_c$), where the coherent length is no longer the Nekhoroshev time but a characteristic time of the phase fluctuation defined by Eq. (2·30). To complete the parallelism mentioned above it is necessary to describe the fluctuation of the characteristic frequency in the sub-critical regime as well as in the stagnant layer.

What we have discussed in the present paper is the stagnant effects originated only from the critical regime between chaos and torus, that is usually a very narrow band in phase space. But we have to understand the stagnant motions in the more wide view, namely, the stagnant motions should be classified into a certain group which reveals the weak ergodicity, and it must be characterized independently free from the KAM theory. The following is an example which has no KAM tori in phase space,

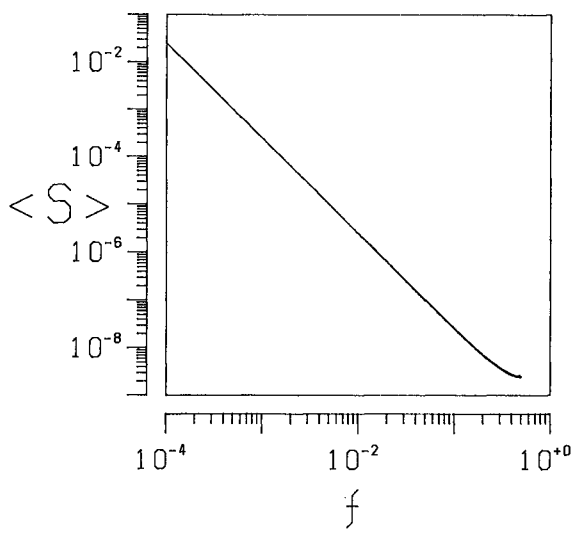

Fig. 8. The f^{-2} power spectrum of X-variable in the weakly ergodic system of Eq. (8·2) with $B=10^{-4}$.

$$X'=X+Y^B,$$
$$Y'=Y+X', \quad (\text{mod. } 1) \tag{8·2}$$

where B is a parameter ($0<B$); the Arnold cat map for $B=1$, and the

one-dimensional torus for $B=0$ or $B=\infty$. The point is that the modified cat map has the C-system property for $0<B<\infty$. As the stable and unstable manifolds of the fixed point can be tangential but the perpetual stablility is guaranteed almost everywhere in the phase space, the motions are very sticky in the limit for $B\to 0$ or $B\to\infty$. Then the entropy is decreasing to zero and the PSD function reveals the f^{-2} spectrum as is shown in Fig. 8. The categorization of such weak ergodic class will be discussed elsewhere.

Acknowledgements

It is a great pleasure for the present authors to dedicate this paper to Professor Nobuhiko Saito on the occasion of his retirement from Waseda University. The authors thank him for valuable discussions and continuous encouragement.

References

1) H. Poincaré, *Les Methodes Nouvelles de la Mechanique Celeste* (Gauthier-Villars, Paris, 1982) or reprint (Dover, N. Y., 1957).
2) V. K. Mel'nikov, Trans. Moscow Math. Soc. **12** (1963), 1.
3) V. I. Arnold, Sov. Math. Dokl. **5** (1964), 581.
4) S. Smale, Bull. Am. Math. Soc. **73** (1967), 747.
5) D. V. Anosov, Sov. Math. Dokl. **4** (1963), 1153.
6) Ya. G. Sinai, Funct. Anal. Appl. **2** (1968), 61.
7) V. I. Oseledec, Trans. Moscow Math. Soc. **19** (1968), 197.
8) Ja. B. Pesin, Sov. Math. Dokl. **17** (1976), 196.
9) V. I. Arnold, Russ. Math. Surveys **18:6** (1963), 85.
10) E. T. Whittaker, *A Treatise on the analytical dynamics of particles and rigid bodies* (Camb. Univ. Press, Cambridge, 1964).
11) I. E. Farquhar, *Ergodic Theory in Statistical Mechanics* (Interscience Publ., N. Y., 1964).
12) E. Fermi, Z. Phys. **24** (1923), 261.
13) Y. F. Chang, M. Tabor and J. Weiss, J. Math. Phys. **23** (1982), 531.
14) M. Tabor, *Chaos and Integrability in Nonlinear Dynamics* (John-Wiley & Sons, N. Y., 1989).
15) S. L. Ziglin, Funct. Anal. Appl. **16** (1983), 181; **17** (1983), 6.
16) H. Yoshida, Physica **29D** (1987), 128; Commun. Math. Phys. 116(1988), 529.
17) A. N. Kolmogorov, Proc. 1954 Int. Cong. of Math. **1** (1954), 315.
18) R. Abraham and J. E. Marsden, *Foundations of Mechanics* (Benjamin-Cummings, N. Y., 1978).
19) P. Billingsley, *Ergodic Theory and Information* (John-Wiley, N. Y., 1965).
20) J. K. Moser, Memoirs Amer. Math. Soc. **81** (1968), 1.
21) V. I. Arnold and A. Avez, *Ergodic Problems of Classical Mechanics* (Benjamin, N. Y., 1968).
22) C. L. Siegel and J. Moser, *Lectures on Celestial Mechanics* (Springer, N. Y., 1971).
23) J. K. Moser, *Stable and Random Motions in Dynamical Systems* (Princeton Univ. Press, N. Y., 1973).
24) A. J. Lichtenberg and M. A. Lieberman, *Regular and Stochastic Motion* (Springer, N. Y., 1982).
25) E. Zehnder, Commun. Pure Appl. Math. **26** (1973), 131.
26) G. D. Birkhoff, Acta Mathematica **50** (1927), 359; *Dynamical Systems* (Am. Math. Soc., N. Y., 1927).
27) B. V. Chirikov, Phys. Rep. **52** (1979), 263.
28) D. F. Escande, Physica Scripta **T2:1** (1982), 126; Phys. Rep. **121** (1985), 165.
29) A. Ollongren, B. A. N Netherland **16** (1962), 241.
30) M. Hénon and C. Heiles, Astron. J. **69** (1964), 73.
31) G. Contopoulos, J. Math. Phys. **7** (1966), 788.
32) B. Barbanis, Astron. J. **71** (1966), 415.

33) I. M. Gel'fand, M. I. Graev, N. M. Zueva, M. S. Mikhailova and A. I. Morozov, Sov. Phys. Dokl. **7** (1962), 223.
34) M. N. Rosenbluth, R. Z. Sagdeev, J. B. Taylor and G. M. Zaslavski, Nucl. Fusion **6** (1966), 297.
35) G. H. Walker and J. Ford, Phys. Rev. **188** (1969), 416.
36) Y. Aizawa and N. Saito, J. Phys. Soc. Jpn. **32** (1972), 1636.
37) Y. Aizawa, J. Phys. Soc. Jpn. **33** (1972), 1693.
38) J. Ford and G. H. Lunsford, J. Math. Phys. **13** (1972), 700.
39) J. N. Mather, Commun. Math. Phys. **86** (1982), 465; Erg. Theory and Dyn. Sys. **4** (1984), 301.
40) A. B. Katok, Erg. Theory and Dyn. Sys. **2** (1982), 185.
41) S. Aubry, Physica **7D** (1983), 240.
42) R. S. Mackay and I. C. Percival, Commun. Math. Phys. **98** (1985), 469.
43) D. Ruelle, *Thermodynamical Formalism* (Addison-Wesley, N. Y., 1978).
44) R. Bowen, Springer lecture note in Math. **470** (1975), 1.
45) Ya G. Sinai, Russ. Math. Surveys **27:4** (1972), 21.
46) B. B. Mandelbrot, *Fractals, Form, Chance, and Dimensions* (W. H. Freeman, San Francisco, 1977).
47) K. G. Wilson, Rev. Mod. Phys. **47** (1975), 773 and references cited therein.
48) M. Feigenbaum, J. Stat. Phys. **21** (1979), 669.
49) J. M. Greene, J. Math. Phys. **20** (1979), 1183.
50) J. M. Greene, R. S. MacKay, F. Vivaldi and M. J. Feigenbaum, Physica **3D** (1981), 468.
51) D. F. Escande and F. Doveil, J. Stat. Phys. **26** (1981), 257.
52) D. F. Escande, Physica **D6** (1982), 119.
53) S. J. Shenker and L. P. Kadanoff, J. Stat. Phys. **27** (1982), 631.
54) R. S. MacKay, Physica **7D** (1983), 283.
55) R. S. MacKay, J. D. Meiss and I. C. Percival, Physica **13D** (1984), 55.
56) P. J. Holmes and J. E. Marsden, J. Math. Phys. **23** (1982), 669.
57) D. Bensimon and L. P. Kadanoff, Physica **D13** (1984), 82.
58) T. Hatori and H. Irie, Prog. Theor. Phys. **78** (1987), 249.
59) D. K. Umberger and J. D. Farmer, Phys. Rev. Lett. **55** (1985), 661.
60) Y. Aizawa, Prog. Theor. Phys. **71** (1984), 1419.
61) G. D. Birkhoff, Proc. N. A. S. **17** (1931), 650, 657.
62) G. D. Birkhoff and P. A. Smith, J. Math. Pure Appl. **9** (1928), 345.
63) Ya G. Sinai, *Introduction to Ergodic Theory* (Princeton Univ. Press, 1976).
64) W. Parry, *Topics in Ergodic Theory* (Camb. Univ. Press, Cambridge, 1981).
65) P. Walters, *An introduction to Ergodic Theory* (Springer, 1982).
66) A. G. Kusinirenko, Sov. Math. Dokl. **6** (1965), 360.
67) R. Bowen and D. Ruelle, Invent. Math. **29** (1975), 181.
68) R. S. Ellis, *Entropy, large deviations, and statistical mechanics* (Springer, 1985).
69) Y. Takahashi, *Dynamical systems and applications,* ed. N. Aoki (World Sci., Singapore, 1987), p. 1.
70) N. N. Nekhoroshev, Russ. Math. Surveys **32** (1977), 1.
71) G. Benettin and G. Gallavotti, J. Stat. Phys. **44** (1986), 293.
72) B. Benettin, *Nonlinear evolution and chaotic phenomena,* ed. G. Gallavotti and P. F. Zweifel (NATO ASI series B, Phys. vol. 176; Plenum press, N. Y., 1988), p. 121.
L. Galgani, ibid. p. 147.
A. Giorgilli, ibid. p. 161.
73) E. Fermi, J. Pasta and S. Ulam, *Fermi's collected works* **2** (Univ. Chicago Press, 1965).
74) J. Ford and J. Waters, J. Math. Phys. **4** (1963), 1293.
75) E. A. Jackson, J. Math. Phys. **4** (1963), 551.
76) F. M. Israiliev and B. V. Chirikov, Sov. Phys-. Dokl. **11** (1966), 30.
77) H. Hirooka and N. Saito, J. Phys. Soc. Jpn. **26** (1969), 624.
78) N. Saito, N. Ooyama, Y. Aizawa and H. Hirooka, Prog. Theor. Phys. Suppl. No. 45 (1970), 209.
79) G. Gallavotti, *Scaling and self-similarity in physics,* ed. J. Frölich (Birkhauser, Boston, 1983).
C. E. Wayne, Commun. Math. Phys. **96** (1984), 311, 331.
80) D. N. Payton, M. Rich and W. M. Visscher, Phys. Rev. **160** (1967), 706.

81) M. C. Carotta, C. Ferrario, G. Lo Vecchio and L. Galgani, Phys. Rev. **A17** (1978), 786.
82) L. Galgani and G. Lo Vecchio, Nuovo Cim. **52** (1979), 1.
83) J. M. Petit and M. Hénon, Icarus **66** (1986), 536.
84) M. Toda, Phys. Rep. **18** (1975), 1.
M. Hénon, Phys. Rev. **B9** (1974), 1921.
85) Y. Aizawa, Prog. Theor. Phys. **81** (1989), 249.
86) B. B. Mandelbrot, SIAM Review **10** (1968), 422.
87) S. Taqqu, Colloquia Mathematics Societatis Jauos Bolyai 27, Random Fields, Esztergon (Hungary, 1977), 1057.
88) D. W. Allan, Proc. IEEE **54** (1966, Feb.), 221 and *Frequency Stability*, ed. Venceslav F. Kroupa (IEEE Press, N. Y., 1983).
89) Y. Aizawa, C. Murakami and T. Kohyama, Prog. Theor. Phys. Suppl. No. 79 (1984), 96.
90) W. Feller, *An Introduction to Probability Theory and Its Application* (John Willey, 1966), vol. 2.
91) D. R. Cox and H. D. Miller, *The Theory of Stochastic Processes* (Methuen & Co. Ltd., 1965).
92) L. A. Bunimovich and Ya G. Sinai, Commun. Math. Phys. **78** (1980), 247; **78** (1981), 479.
93) B. J. Alder and T. E. Wainwright, Phys. Rev. **1A** (1970), 18.
94) H. van Beijieren, Rev. Mod. Phys. **54** (1982), 195.
95) G. Casati, G. Comparin and I. Guarneri, Phys. Rev. **26A** (1982), 717.
96) J. Machta, J. Stat. Phys. **32** (1983), 555.
97) F. Vivaldi, G. Casati and I. Guarneri, Phys. Rev. Lett. **51** (1983), 727.
98) C. F. F. Karney, Physica **8D** (1983), 360.
99) T. Kohyama, Prog. Theor. Phys. **71** (1984), 1104.
100) L. A. Bunimovich, Commun. Math. Phys. **65** (1979), 295.
101) G. Benettin and J. M. Strelcyn, Phys. Rev. **17A** (1978), 773.
102) A. Zacherl, T. Geisel, J. Nierwtberg and G. Radon, Phys. Lett. **114A** (1986), 317.
103) J. P. Bouchaud and P. Le Doussal, J. Stat. Phys. **41** (1985), 225.
104) T. Geisel, *Synergetics, Order and Chaos,* ed. M. G. Velarde (World Sci., Singapore, 1988), p. 601.
105) J. D. Hanson, J. R. Cary and J. D. Meiss, J. Stat. Phys. **39** (1985), 327.
106) P. Manneville, J. de Phys. **41** (1980), 1235.
107) Y. Pomeau and P. Manneville, Commun. Math. Phys. **74** (1980), 189.
108) I. Procaccia and H. Schuster, Phys. Rev. **A28** (1983), 1210.
109) Y. Aizawa, Prog. Theor. Phys. **70** (1980), 1249.
110) T. Kohyama and Y. Aizawa, Prog. Theor. Phys. **71** (1984), 917.
111) Y. Aizawa and T. Kohyama, Prog. Theor. Phys. **71** (1984), 847.
112) Y. Aizawa, Prog. Theor. Phys. **72** (1984), 659.
113) M. Hénon, Q. J. Appl. Math. **27** (1969), 291.
114) I. Procaccia, *Dimensions and Entropies*, ed G. Mayer-Kress (Springer, 1986), p. 8.
115) T. Kohyama, Dr. Thesis (Kyoto University, 1986).
116) Many references in *Hamiltonian Dynamical Systems* compiled by R. S. MacKay and J. D. Meiss (Adam Hilger, Bristol and Philadelphia, 1987).
117) M. Donsker and S. R. S. Varadhan, Commun. Pure Appl. Math. **28** (1975), 1.
118) A. Rényi, Rev. Inst. Internat. Stat. **33** (1965), 1.
119) T. Konishi, this issue, p. 19.
120) Y. Aizawa and Y. Kikuchi, *The study of Dynamical Systems,* ed. N. Aoki (World Sci. Singapore, 1989), in press.